Annu. Rev. Nucl. Part. Sci. 1991. 41: 219–67

LOW ENERGY ANTIPROTON PHYSICS

Claude Amsler

Physik-Institut der Universität Zürich, Schönberggasse 9, CH-8001 Zürich, Switzerland

Fred Myhrer

Department of Physics, University of South Carolina, Columbia, South Carolina 29208, USA

KEY WORDS: antiproton scattering, antiproton-proton annihilation, meson spectroscopy, antiproton-nucleus

CONTENTS

1. INTRODUCTION

This report summarizes the present experimental and theoretical status of antinucleon-nucleon ($\bar{N}N$) interactions at low energy (below 2 GeV/c). We discuss elastic scattering, hyperon pair production, and annihilation into mesonic channels, including the search for exotic meson states in the annihila-

0163–8998/91/1201–0219$02.00

tion debris. New results from the Low Energy Antiproton Ring (LEAR) at CERN, from KEK in Japan, and from Brookhaven National Laboratory (BNL) are now available. Some of the experiments and their comparison to theoretical predictions have been reviewed earlier (1–3). We extend these reviews to more recent data and theoretical calculations.

Before discussing low energy $\bar{N}N$ interactions, it should be emphasized that the physics is based on models, as is most of strong interaction physics. Presumably, the theory of quantum chromodynamics (QCD) describes the strong force between quarks and gluons. At low energy and low momentum transfer, the QCD coupling constant becomes large and could lead to color confinement of quarks. A picture of the baryon structure has emerged from our present knowledge of QCD. At large distances the quarks feel the confinement forces, while at short distances they are almost free; thus their interactions can be treated perturbatively. This is the basis for phenomenological models like the MIT bag model (4) or the nonrelativistic quark model in which confinement is simulated by an harmonic oscillator potential (5, 6). Both models successfully describe the baryon mass differences, the excited baryon mass spectra, the baryon magnetic moments, etc, where the few model parameters are fixed by reproducing the proton mass, the nucleon-Δ mass difference, and the Λ mass. Low energy strong interactions are guided by the requirements of chiral symmetry, which, when incorporated into the bag model, describes the nucleon as a core of three confined valence quarks surrounded by a cloud of pions (7, 8). The pions are distributed around the quark core in a manner dictated by chiral symmetry. As a consequence, the observed root mean square (rms) charge radius of the proton (0.9 fm) is larger than that of the quark core because of the corrections from the pion cloud.

When using this model to describe the $\bar{N}N$ interactions, it becomes clear that the quark core and the pion cloud participate differently in $\bar{N}N$ reactions. When only the pion clouds overlap (large $\bar{N}N$ impact parameters), long-range meson exchanges are expected to describe the process. However, for S-wave scattering (zero-impact parameter), both meson exchanges and quark-antiquark interactions contribute to the scattering process as a result of the overlapping cores. In this picture, annihilation occurs only when the quark cores overlap, which means that annihilation takes place at $\bar{N}N$ distances somewhat shorter than the pion Compton wavelength.

For $\bar{N}N$ scattering (elastic $\bar{p}p$, $\bar{p}n$, and charge exchange $\bar{p}p \rightarrow \bar{n}n$), all annihilation channels contribute to the inelasticity. This means that only the dominant bulk properties of annihilation are needed to treat the loss of flux from the $\bar{N}N$ scattering channels. The long-range part of the $\bar{N}N$ potential is determined from the NN meson exchange potential. The only

requirement is that the exchanged mesons of odd G parity (π and ω) must have opposite sign in the $\bar{N}N$ potential. In some $\bar{N}N$ models a complex short-range potential is added to simulate the annihilation processes (9, 10) and the sizes of the hadrons themselves. Another model assumes meson exchanges at large distances and an absorptive boundary condition at short distances ($R \approx 0.5$ fm) (11). In all these models the long-range $\bar{N}N$ meson exchange potential (MEP) is very attractive and pulls the $\bar{N}N$ wave function into the annihilation region. The net effect is that the effective absorption radius (R_{eff}) is larger than the radius of the absorptive boundary condition. As a consequence, the forward slope of the elastic differential cross section (and its energy dependence) is given by the MEP (12). In other words, the forward low energy $\bar{N}N$ scattering ($p_{\text{lab}} < 800$ MeV/c) is dominated by MEP. Thus the longer range (real part) of the $\bar{N}N$ potential is playing a significant role, which can be studied in $\bar{p}p$ scattering. These models describe the forward differential cross sections well. They do not, however, fit the angular and energy dependence of recent $\bar{p}p$ polarization data from LEAR. The new scattering data are so precise that one can test some basic aspects of these models and possibly gain further insight into the scattering process. One should keep in mind that NN scattering above $p_{\text{lab}} = 1.5$ GeV/c is mainly diffractive (13), so we expect $\bar{N}N$ to become diffractive at a somewhat lower energy. Hence the MEP description is not useful above about 1 GeV/c.

It should also be stressed that, even at very low momenta, elastic $\bar{p}p$ scattering requires more partial waves than its pp counterpart. Because of the strong absorption of the $\bar{p}p$ S wave (quark cores overlap), the dominant partial waves are the P waves, and some D waves are already required at 300 MeV/c (14). This is in contrast to pp scattering, which is dominated by S waves at the same momentum. Furthermore, all phase shifts are complex because of annihilation, and both isospin 0 and 1 contribute in each partial wave. Hence a treatment of $\bar{p}p$ scattering is intrinsically more complex than for the familiar NN system. The experimental information at low energy is still quite fragmentary, with only differential cross sections being measured down to 180 MeV/c (14).

At low momentum, the annihilation cross section is very large and exceeds the elastic cross section. The study of the annihilation process might give new insight into the physics of hadronization. At high energy, multiparticle production dominates the total cross section. Thus high energy multiparticle production and low energy annihilation processes can be considered complementary studies of hadronization. The high energy production seems to be dominated by the dynamics of stretching color-flux tubes, which hadronize into jets, as in the Lund model (15). In contrast, low energy $\bar{N}N$ annihilation can be thought of as generating a hot, con-

centrated quark gas of energy ~ 2 GeV that subsequently evaporates into an average of five pions. In fact, some aspects of $\bar{p}p$ annihilation seem to follow from a statistical thermodynamical description. In this respect, $\bar{p}p$ low energy studies are small-scale versions of high energy heavy-ion experiments searching for the quark-gluon plasma, which many anticipate will be observed at the planned relativistic heavy-ion collider (RHIC) at BNL.

While the statistical models successfully describe the final-state pion multiplicity distribution and branching ratios of in-flight $\bar{p}p$ annihilation, they are not designed to fit the branching ratios for annihilation at rest into two or three meson resonances from specific $\bar{p}p$ atomic states. Some two- and three-body meson final states have recently been investigated at LEAR and KEK for $\bar{p}p$ annihilation at rest. The angular momentum of the initial $\bar{p}p$ atomic states, following $\bar{p}$ capture in hydrogen, can be determined by measuring the atomic x rays in coincidence with the final mesons. Here the annihilation process is studied under controlled circumstances that contrast with the dynamical hadronization process associated with jet production. A strong dependence on the initial angular momentum is observed, and current QCD-inspired model calculations fail to reproduce the measured branching ratios satisfactorily.

Antiproton-proton annihilation at low energy is also a tool to investigate the production of meson resonances with masses below 2 GeV. Apart from the standard $\bar{q}q$ states, one can produce exotic mesons such as a two-quark–two-antiquark $\bar{q}^2q^2$ or other multiquark mesons as well as hybrid mesons, for example $\bar{q}qg$, or glueballs (mesons made exclusively of gluons, g). Speculations based on various models predict the existence of such exotic mesons, but none has been convincingly observed in any hadronic reaction, although several candidates exist (for reviews, see 16, 17). In $\bar{p}p$ annihilation, the LEAR experiments have not observed any narrow baryonium (quasi-nuclear $\bar{N}N$) states, but broad states are not excluded (18). Relevant data on exotic mesons have been hindered by the lack of statistics and by the lack of detectors capable of precisely reconstructing exclusive final states involving kaons and neutral mesons like π^0's and η's. With the Crystal Barrel, Jetset, and Obelix detectors, which are on the floor at LEAR, there is for the first time a reasonable chance of observing an exotic meson. We review in this report the LEAR results pertaining to the existence of such exotic states.

2. ANTINUCLEON-NUCLEON SCATTERING

At low energies ($p_{lab} < 1$ GeV/c), the forward $\bar{p}p$ scattering processes (elastic and charge exchange $\bar{p}p \rightarrow \bar{n}n$) are described by the long-range

meson exchanges, supplemented by models or parametrizations for $\bar{p}p$ annihilation (which is effective at $\bar{N}N$ relative distances of 0.6 to 1.4 fm in most models). The Schrödinger equation with the meson exchange potential (MEP) and a parametrization for the annihilation (often an optical potential) is solved to ensure that unitarity is satisfied when the observables are calculated. We present these ideas and then examine the experimental evidence that supports them.

2.1 *Theoretical Considerations*

2.1.1 THE MESON EXCHANGE FORCES The long-range meson exchange potentials include one-pion exchange, two-pion exchange, ω exchange, and the short-distance nuclear forces.

The one-pion-exchange (OPE) potential is well tested in nuclear physics (see Figure 1). It describes the higher NN scattering partial waves (20) and the deuteron asymptotic D/S ratio (21). In both cases the pion and the nucleons are treated as pointlike particles. The pion-nucleon coupling constant is well known, $g^2_{\pi NN}/4\pi \simeq 14.4$. Since the tensor part of the OPE potential behaves as r^{-3} at short distances, a cutoff is needed in practical calculations (a natural cutoff is the structure of the nucleon and pion).

The two-pion-exchange (TPE) potential (Figure 1) is calculated using dispersion theory by the Paris (22) and the Stony Brook (23) groups. Part of the TPE potential is also calculated by the Bonn group in an effective field theory (24). This TPE potential is simulated in one-boson exchange potentials (OBEP) by isoscalar-scalar and isovector-vector (ρ meson) ex-

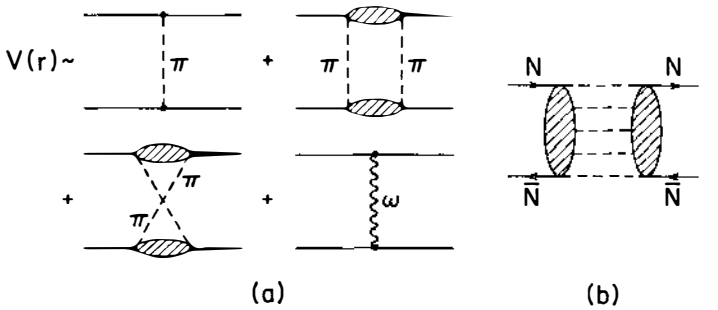

Figure 1 (*a*) Illustration of the one-pion, two-pion, and ω exchange potentials. The shaded ellipses for two-pion exchange are calculated in dispersion theory using as input pion-nucleon and pion-pion scattering data. For a recent review see (19). (*b*) The process $\bar{N}N \rightarrow$ intermediate meson states $\rightarrow \bar{N}N$, illustrating that many intermediate meson states contribute to $\bar{N}N$ scattering via unitarity.

changes. Because of its large width, the ρ is included in TPE in a more natural way as a "bare" $\bar{q}q$ state embedded in the two-pion continuum, which has a range of $(2m_\pi)^{-1}$ or less. The TPE potential is not tested to high accuracy in NN scattering.

The ω exchange potential is assumed to give the NN repulsion in most meson exchange models. However, the value of the omega-nucleon coupling constant g_ω is very uncertain. We expect from SU(3) and vector-meson dominance $g_\omega^2/4\pi$ to be 4.5 (25), but in meson exchange models, like the Paris model, one needs a value of 10 to 12 to fit NN data. Be aware that cutoffs (or short-distance parametrizations) play a role in determining the latter values, as we discuss next.

The short-distance nuclear forces are often parametrized with (arbitrary) form factors (cutoffs). For short distances, it is difficult to separate the physics of a form factor from two or more meson exchanges. Many NN potential models introduce a short distance cut-off parametrization instead of form factors (22, 26). Some OBEP models also include heavier meson exchanges that we do not consider here. During the last ten years, model calculations have shown that most of the NN repulsion can be explained by using the Pauli principle on the quark level (with some help from the color-magnetic quark forces, which contribute to the nucleon-Δ mass difference). The quark degrees of freedom give S waves and $^1P_1$ NN phase shifts similar to hard-core phase shifts as a function of energy (19, 27). Model agreement with data is impressive. Including an ω exchange with a modest $g_\omega^2/4\pi = 4.5$ does not change the results of these phase-shift calculations. The quark model results are still being debated.

An $\bar{N}N$ potential can be generated from the one-pion, two-pion, and ω NN meson exchange potentials described above if one uses G-parity arguments (9, 28). This gives a good description for large $\bar{N}N$ separations. It generates a strongly attractive long-range force and, as we discuss below, it describes the $\bar{N}N$ forward differential cross-section data. However, the meson exchanges between nucleons implicitly assume pointlike nucleons and mesons. In NN OBEP, a form factor of $\sim(q^2+\Lambda^2)^{-1}$ is used with $\Lambda \sim 1.0$–1.5 GeV to parametrize the short-distance potentials (24), whereas the chiral or cloudy bag models of the nucleons give a "softer" πNN form factor (7, 8). This parametrization of the short-distance NN potentials should not be directly transferred to $\bar{N}N$ and there is a good reason for using quark models to describe these short-distance potentials: for NN and $\bar{N}N$ separations less than 1 fm, the quark cores are expected to overlap. Quark degrees of freedom for short-distance forces naturally lead in $\bar{N}N$ to annihilation processes, discussed in the next subsection.

A final comment on meson exchange forces: Theoretical calculations of NN or $\bar{N}N$ interactions should show how the observables change when

the values of the cutoff parameters in the various potentials are changed. In this way one may better judge which parts of the calculations reflect the physics input.

2.1.2 THE ANNIHILATION AND $\bar{N}N$ SCATTERING To describe $\bar{N}N$ scattering observables we need, as alluded to above, a model for the annihilation process (see Sections 3.3 and 3.4). In $\bar{p}p$ scattering, annihilation occurs when the $\bar{N}$ and N quark cores overlap. For chiral bag models, the nucleon quark core has an rms radius of 0.65 to 0.75 fm; we thus expect annihilation to be effective at $\bar{N}N$ distances of 1 fm or less. The annihilation model is therefore intimately tied to the short-distance forces discussed above. For scattering processes, only the bulk properties of annihilation contribute through unitarity to $\bar{N}N$ scattering, where we have to sum over all intermediate meson channels. The processes shown in Figure 1*b* can be described by optical potentials constructed so that unitarity is satisfied in the scattering process. We have only a primitive model-dependent understanding of the annihilation process itself, but since the many competing annihilation channels have to be added, it is reasonable to assume that the sum will have no strong spin nor isospin dependence.

The following models support our belief that the spin and isospin dependences indeed average out. The simplest model to describe the bulk properties of annihilation is the hot gas model (29). The energy spectrum of the pions in the annihilation reaction $\bar{p}p \to \pi^{\pm} +$ anything is well described by a hot gas with a temperature of $T \sim 100$ MeV. As a consequence of this model, we expect quantum numbers to be distributed in a statistical manner, as reinforced by the isospin statistical model (30). This model, which has been confirmed experimentally for $\bar{p}p$ annihilating into pions (31), says that for a given number of pions n in the final state, the cross-section ratios of the different charged channels (for instance for $n = 5$, the channels $2\pi^+2\pi^-\pi^0$ or $\pi^+\pi^-3\pi^0$ or $5\pi^0$) are determined by a statistical distribution in the pion charges according to the weight $(n_{\pi^+}!n_{\pi^-}!n_{\pi^0}!)^{-1}$, where $n = n_{\pi^+} + n_{\pi^-} + n_{\pi^0}$. Finally, in the threshold dominance model, recently elaborated by Vandermeulen (32), the energy dependence of the cross sections for $\bar{p}p$ into two or more pions is fitted with two parameters. The model averages over spin and isospin of the intermediate two-meson channels leading to the same final state. We discuss these models in some detail in Section 3.3.

Another feature of annihilation is based on dispersion arguments (33), which say that the annihilation forces should be of short range, approximately $\exp(-2Mr)/r$, where M is the nucleon mass and r is the relative $\bar{N}N$ distance (9, 10, 34, 35) (see Figure 1*b*). On the quark level, model calculations also find a rapid damping of the annihilation strength with

increasing r for distances larger than 0.7 fm (36). In this model the absorption is so strong that for $r < 0.7$ fm $\bar{N}N$ scattering becomes insensitive to the short-distance ($r < 0.7$ fm) potential behavior and hence absorption is complete (the wave function becomes zero) at very short $\bar{N}N$ distances. An extreme model simulates annihilation by a black sphere of radius R, which, together with MEP, fits data for $R \approx 0.5$ fm (11). The black sphere effectively absorbs all low impact parameter $\bar{N}N$ scattering.

Other types of models for annihilation used in $\bar{N}N$ scattering are based on an effective meson-baryon theory that implicitly assumes pointlike particles. Annihilation is described by baryon exchanges in which $\bar{N}N$ couples to two mesons (37–39). These baryon exchanges correspond to Yukawa forces with a range of the order of $(2M)^{-1}$, which is small compared to the rms radii of the baryons themselves, a point we elaborate on in the next subsection. In a coupled-channel calculation the $\bar{N}N$ wave function is nonzero at very small distances, contrary to the optical models (39). These approaches introduce vertex form factors that also have ranges of the order of the inverse nucleon mass. One question is whether this coupled-channel description can be a reasonable parametrization of the successful Vandermeulen model (32) in which heavy intermediate mesons (ω, ρ, a_0, a_1, f_0, K*, ϕ, etc) are needed and dominate (see Section 3.3). Some of these intermediate states have been incorporated in recent distorted wave Born approximation (DWBA) calculations by the Jülich group (40).

2.1.3 BARYONIUM AND ANNIHILATION In the original work of Shapiro and collaborators, $\bar{N}N$ resonances and bound states were predicted on the basis of the strongly attractive meson exchange potential (41). We refer to these molecular $\bar{N}N$ states as quasi-nuclear or baryonium states. On the other hand, $\bar{q}^2q^2$ Regge trajectories are also predicted, for which the intercepts and slopes have been determined (42). The $\bar{N}N$ potential trajectories (which are not straight lines) are very sensitive to the short-range parametrization of the potential, which introduces uncertainties large enough for the $q^2\bar{q}^2$ and the isospin zero $\bar{N}N$ trajectories to coincide around the $\bar{N}N$ threshold (43). Hence baryonium states are difficult to distinguish from pure $\bar{q}^2q^2$ states.

It was argued by many that the coupling to the annihilation channels was weak. This implies that one should observe narrow $\bar{N}N$ states. However, any $\bar{N}N$ model that described scattering cross sections required annihilation to be effective at 1 fm $\bar{N}N$ separation, despite having a short Yukawa range (44–47); this requirement made the $\bar{N}N$ states very broad.

The crucial argument of Shapiro leading to narrow baryonium states was based on meson-baryon dispersion theory (48, 49) (see Figure 1*b*). He

and his collaborators argued that annihilation due to baryon exchange had to be of very short range and they therefore concluded that annihilation is weak at $\bar{N}N$ separation of 1.0–1.5 fm, which is the typical size of an $\bar{N}N$ state calculated from the many meson exchange potentials, neglecting annihilation. The flaw in this line of argument is that a nucleon has a sizeable quark core and these quarks are confined. Quark confinement implies that dispersion theory arguments do not readily apply to quark degrees of freedom. If, as indicated by quark models, the baryon Compton wavelength is much smaller than the quark confinement radius, the latter determines the shortest $\bar{N}N$ distance down to which the dispersion arguments apply.

2.2 *Scattering Experiments*

2.2.1 INTEGRATED CROSS SECTIONS The $\bar{p}p$ cross sections—total (50, 51), elastic (14), annihilation (52), and charge exchange (53)—have all been measured at LEAR energies down to $\sim$200 MeV/c. The Obelix collaboration has even measured the annihilation cross section at 70 MeV/c (54). At low energy ($\sim$300 MeV/c), the annihilation cross section exceeds the elastic cross section by a factor of two.

As is evident from the measured elastic differential cross section at $p_{lab} = 180$ MeV/c, the P wave is important. Because of the strong S-wave absorption, the imaginary parts of the S-wave amplitudes are close to their unitarity limit $\sim 1/2k$ (where $k \approx p_{lab}/2$ is the center-of-mass momentum). For $p_{lab} \approx 180$ MeV/c, P waves already contribute approximately 40% of the total cross section (14) in contrast to $\sim$10% in pp. (The strong P wave is caused by the strongly attractive MEP, which pulls the $\bar{N}N$ wave function into the shorter-range absorption region). As discussed recently by Kroll & Schweiger (55), to reflect the importance of the P waves, the total cross section at LEAR energies should be parametrized as

$$\sigma_{tot}(\text{mb}) = 108.4/k + 13.5 + 187k + 495k^2 - 784k^3 + \cdots, \qquad 1.$$

where the center-of-mass momentum k is in units of fm^{-1}. At $p_{lab} = 180$ MeV/c the center-of-mass momentum is $k \simeq 0.46$ fm^{-1}. For much lower values of k, the two last terms in Equation 1 can be dropped. However, it is obviously a very bad approximation to drop both the third term, which comes from the P waves, and the last two terms in Equation 1 for $p_{lab} \geq 180$ MeV/c. Unfortunately, the total cross section has been approximated by the empirical formula

$$\sigma_{tot}(\text{mb}) = 54/p_{lab}(\text{GeV}/c) + 66 \qquad 2.$$

as quoted in the review by Walcher (1). This last formula should no longer be used. The annihilation cross section is empirically given by (52)

$$\sigma_a(\text{mb}) = 46.6/p_{lab}(\text{GeV}/c) - 30.1 + 60.3p_{lab}(\text{GeV}/c). \quad 3.$$

The annihilation cross section exceeds the unitarity limit for an S wave at 200 MeV/c by a factor 1.7, requiring a strong P wave.

Originally, these cross sections were measured to search for resonances of the $\bar{p}p$ system. The controversy on the existence of $N\bar{N}$ resonances has been settled at LEAR (for a review, see 18). The $\bar{p}p$ total cross section does not show any evidence for either broad or narrow states below 1 GeV/c. For narrow states ($\Gamma < 3.5$ MeV) the upper limit for the integrated cross section is 2 mb MeV above 400 MeV/c (50) and 8 mb MeV between 220 and 400 MeV/c (51). No structure (with an upper limit of 5 mb MeV) is observed in the inclusive annihilation cross section between 400 and 600 MeV/c (56). For limits on $\bar{N}N$ bound states, see Section 3.1.5.

2.2.2 ELASTIC SCATTERING The elastic $\bar{p}p$ cross section has been measured at LEAR between 180 and 1500 MeV/c (14, 57, 58). The main contribution to the OBEP potential is OPE, with some influence from heavier meson exchanges. The calculated differential cross sections for elastic and charge exchange scattering are shown in Figure 2. They agree with experimental data (1). The forward differential cross section is not sensitive to the precise shape of the annihilation potential. The annihilation potential for the fits of Figure 2 (*left*) was generated from a quark-gluon model and a quark confinement potential (36, 59). A Gaussian annihilation

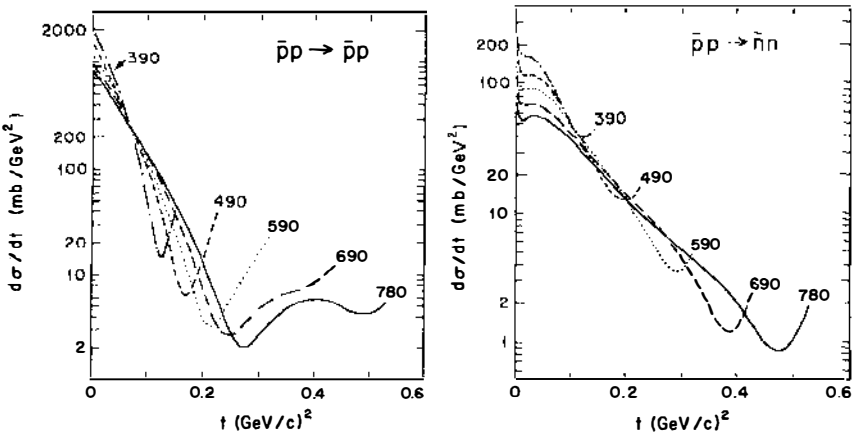

Figure 2 (*Left*) Elastic $\bar{p}p$ differential cross section for various $\bar{p}$ momenta calculated with the Bryan-Phillips potential and the imaginary part constructed from a quark model (36, 59). (*Right*) Charge exchange reaction with the same meson exchange potential but with a black sphere to simulate annihilation (11).

potential (or Woods-Saxon) works equally well and one finds an annihilation radius of 0.7 fm with a depth of ~ 1 GeV (60).

At small angles, the interference of the nuclear and Coulomb amplitudes yields the real part of the (spin-averaged) forward elastic scattering amplitude $f(0)$. The ρ parameter [$\rho = \text{Re}\, f(0)/\text{Im}\, f(0)$] was recently measured at LEAR below 300 MeV/c (61–63) and was discussed by Walcher (1). At zero momentum, ρ is related to the shift and broadening of the $\bar{p}p$ atomic 1S states, which are also measured at LEAR (64). (To be precise, ρ is the ratio of the real to imaginary parts of the hadronic scattering length, while x-ray experiments measure the Coulomb-modified scattering length. The correction is, however, much smaller than the present experimental error.) Using an optical potential, Batty (64) finds from the LEAR x-ray data $\rho = -1.08 \pm 0.09$. Hence ρ must be negative at very low momentum, although scattering data show it to rise toward positive values with decreasing momentum for momenta below 300 MeV/c, which means that ρ must increase very rapidly with increasing momentum very close to threshold. In Kroll & Schweiger's dispersion calculation of the forward $\bar{p}p$ amplitude these measurements of the ρ parameter generate a structure in the imaginary part of the $\bar{p}p$ amplitude ~ 20 MeV below threshold (65). These amplitudes below threshold (55, 65) have been used in a calculation by Fasano & Locher (66), who evaluate the annihilation reaction $\bar{p} + d \rightarrow N + n\pi$, which is sensitive to the imaginary part of the $\bar{p}p$ amplitude below threshold. They conclude that only a weak structure below threshold is compatible with $\bar{p}d$ data.

A fit to low energy cross section and x-ray data, using a coupled-channel effective range expansion of the spin-averaged $\bar{N}N$ S and P waves, shows that the averaged P wave is repulsive and turns attractive below 300 MeV/c, while the averaged S wave remains repulsive (67). Hence the turnover of the ρ parameter at low energy is attributed to this behavior of the P wave.

The $\bar{p}p$ analyzing power $P(\theta)$ has been measured between 439 and 1550 MeV/c (57, 58, 68). In one experimental approach, both proton and antiproton are detected and most of the background from interactions with heavier nuclei in the polarized target is eliminated by angular correlations (57, 68). At low momentum, however, absorption of the proton or antiproton in the target prevents measurements at small and large scattering angles. In another approach, the angle and the energy of one scattered particle (proton or antiproton) are measured in a magnetic spectrometer (58). This method allows coverage of the full angular range. The results from both experiments agree. Figure 3*a* shows $P(\theta)$ at 697 MeV/c compared with model predictions. The agreement is poor but the general trend (dip-bump structures) is reproduced. At lower energies, the $P(\theta)$ predictions in the forward direction are in better agreement with experi-

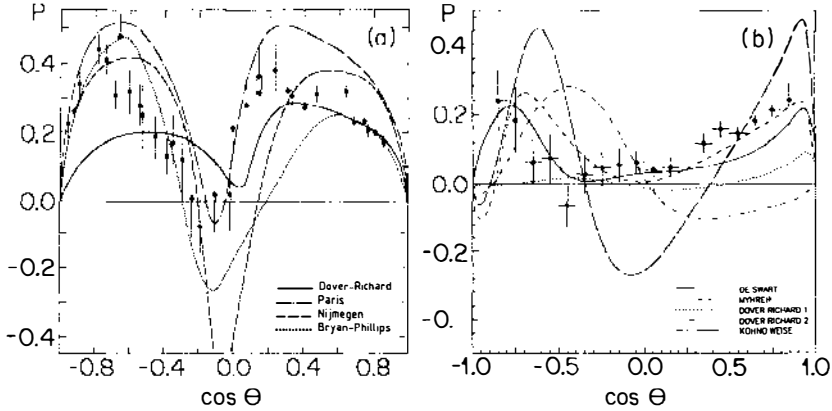

Figure 3 (*a*) Analyzing power $P(\theta)$ for elastic scattering at 697 MeV/c (58) compared with theoretical predictions (9, 10, 34, 69). (*b*) $P(\theta)$ for charge exchange at 656 MeV/c (70) compared with theoretical predictions (10, 11, 60; R. G. E. Timmermans et al, private communication from J. J. de Swart).

ments (71). [Note that the potential of the Nijmegen group (69) has an unphysical long-range phenomenological real part (12, 39).] One main difference between the various theoretical approaches is the short-range assumption for both the real and the imaginary parts of the potential. Hence polarization data, in contrast to cross-section data, are very sensitive to the short-range parametrization (12) and can provide new tests of the various $\bar{N}N$ models.

The measurement of other spin observables (72) is difficult because there are no polarized antiproton beams or suitable analyzers of antiproton polarization. The analyzing power on carbon is very small at low $\bar{p}$ momentum (73). On the other hand, the polarization transfer from the polarized target proton to the recoil proton can only be measured for energetic protons escaping from the target and for which the carbon analyzing power is large. These protons are associated with backward scattered $\bar{p}$, for which the elastic cross section is small. So far we have only a few data points with limited statistics for the depolarization parameter D between (the high momenta) 988 and 1259 MeV/c (74), and the points disagree with theoretical predictions of the low energy models.

2.2.3 CHARGE EXCHANGE The charge exchange $\bar{p}p \rightarrow \bar{n}n$ differential cross section is measured between 180 and 600 MeV/c (53, 70, 75). This cross section is strongly forward peaked, with a shoulder at small momentum transfer, a shape that agrees with OBEP models supplemented by strong annihilation, as discussed by Phillips (28) (see Figure 2*b*). Below

300 MeV/c, earlier data on the total charge exchange cross section (76) showed a much faster increase with energy just above threshold than data from LEAR (53). Also the various data disagree in the experimentally difficult range of extreme forward and backward directions.

Birsa et al measured $d\sigma/d\Omega$ and $P(\theta)$ for this reaction with a polarized penthanol target between 600 and 1300 MeV/c (70). The antineutron is detected by its annihilation in an iron/streamer-tubes calorimeter and the neutron in a scintillation counter array. The target polarization reached a record value of 96%. Figure 3*b* shows the analyzing power at 656 MeV/c together with theoretical predictions.

2.2.4 HYPERON-ANTIHYPERON PRODUCTION The production of $\bar{\Lambda}\Lambda$ pairs in $\bar{p}p \to \bar{\Lambda}\Lambda$ has been studied at LEAR with high statistics close to the $\bar{\Lambda}\Lambda$ threshold (1435 MeV/c) (77, 78). The polarization of the Λ ($\bar{\Lambda}$) is derived from the known self-analyzing power in Λ ($\bar{\Lambda}$) decay into $p\pi^-$ ($\bar{p}\pi^+$). In addition, the spin correlations of the hyperon pairs have been determined at 1546 and 1695 MeV/c (79). The cross section for this reaction rises very quickly from threshold to $\sim$100 μb at $\sim$1650 MeV/c. A trigger was therefore required to collect large statistical samples. This experiment takes advantage of the narrow LEAR $\bar{p}$ beam: the small proton target was surrounded by veto counters to trigger on the emerging hyperon pairs, which have a short decay length.

The main motivation was a study of the $\bar{s}s$ production dynamics, since in a naive constituent quark model, the spin of the s ($\bar{s}$) quark is carried by the Λ ($\bar{\Lambda}$). Again, the S waves are strongly absorbed as a consequence of initial (and final) state interactions, which means that the $L = 0$ amplitude is almost purely imaginary and close to its unitarity limit. As before, we expect the P wave to be important because of the very attractive $\bar{N}N$ potential. A fit to the cross section $\sigma = b_0\varepsilon + b_1\varepsilon^3$ (where $\varepsilon = s^{1/2} - 2m_\Lambda$ and s is the square of the center-of-mass energy) near threshold indeed yields $b_0 = 1.51$ μb/MeV$^{1/2}$ and $b_1 = 0.26$ μb/MeV$^{3/2}$—a dominant S-wave part with an important P-wave part. This is also directly observed from the forward peak in the angular distribution (Figure 4) even at 0.8 MeV above threshold (78). The spin correlation data are consistent with the $\bar{\Lambda}\Lambda$ pair being produced in a pure spin triplet state (79). This is surprising, since in general multiple gluon exchanges and K exchange models (81) predict the spin triplet to dominate, although the spin singlet does not vanish. The spin singlet contribution only vanishes for single-gluon exchange, a questionable approximation at these low energies.

Despite the $\bar{p}p$ high energy, meson exchange potentials have been used here with some success to calculate $d\sigma/d\Omega$ and $P(\theta)$ in a DWBA formulation (81, 82). The main reason for this success is that, close to thresh-

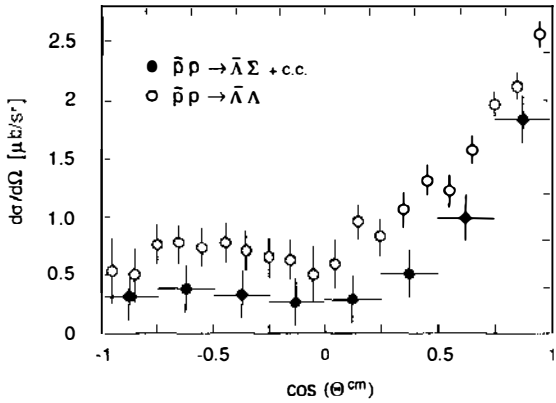

Figure 4 Differential cross section for $\bar{p}p \rightarrow \bar{\Lambda}\Sigma^0$ and $\Lambda\bar{\Lambda}$, each 15 MeV above their respective thresholds (80).

old, only S and P waves contribute. Since S waves for $\bar{p}p \rightarrow \bar{\Lambda}\Lambda$ are almost completely absorbed and the P waves are important, this reaction is sensitive to peripheral meson exchange forces (K exchange) (81). The long-range parts of K and K* t-channel exchanges (and even a naive timelike gluon exchange) give a reasonable fit to the data. However, according to Kohno & Weise (81), close to threshold, $P(\theta)$ is better predicted for only K or a timelike gluon exchange. It should be mentioned that the differential cross section of this peripheral reaction has also been described reasonably well at higher energies ($p_{lab} \simeq 3$ to 6 GeV/c) with just K and K* exchanges, including a Regge-like form factor (83).

The roles of the different reaction mechanisms are being investigated by the same group by studying $\bar{\Lambda}\Sigma^0$ and $\bar{\Sigma}\Sigma$ since in these reactions K exchange is suppressed as a result of the coupling constant inequality $g_{KN\Sigma} \ll g_{KN\Lambda}$. Data for the $\bar{\Sigma}\Sigma$ reaction are not available yet. The angular distributions of the $\bar{\Lambda}$ for $\bar{p}p \rightarrow \bar{\Lambda}\Sigma^0$ and $\Lambda\bar{\Lambda}$, both 15 MeV above their respective thresholds, are very similar (Figure 4). A strong P wave is observed from the forward peak and the ratio of cross sections $\sigma(\bar{\Lambda}\Sigma^0)/\sigma(\Lambda\bar{\Lambda}) = 0.29 \pm 0.02$ agrees well with the prediction from the gluon model of Kohno & Weise (81). Polarization data for the Σ^0 are not yet of sufficient statistical quality to allow a meaningful comparison with theoretical models (80).

2.3 *Antiprotonic Atoms*

In protonium, the strong interaction models discussed above predict the measured 1S energy-level shift with respect to the expected QED value and the total 1S level width. The predicted level shift is typically -0.8 keV

(that is, toward less binding) and the predicted width typically 1.0 keV (64), in good agreement with the experimental averages of -0.72 ± 0.04 and 1.11 ± 0.97 keV respectively (1, 64). So far, there is no measurement of the $^1S_0$ and $^3S_1$ level splitting. The predicted averaged 2P level width in protonium (84, 85) is in reasonable agreement with data. Batty reviewed the $\bar{p}p$ and $\bar{p}d$ atomic cascade measurements (64), and Reifenröther & Klempt presented recently refined cascade calculations (86). All models, which include the neutron-proton mass difference, find that the $\bar{p}p$ atomic wave function is strongly modified at distances $r < 5$ fm. The WKB calculation of Pilkuhn & Kaufmann (84) shows that the OPE potential introduces $\bar{n}n$ components into the atomic wave function, $\psi = a|\bar{p}p\rangle + b|\bar{n}n\rangle$, where $a^2 + b^2 = 1$. All calculations agree that $b \ll a$, but the calculation of Carbonell et al shows that the $|\bar{n}n\rangle$ component is large for $r < 2$ fm, where annihilation takes place (85). This is confirmed by the Aarhus group (87) and by estimates based on scattering lengths made by Jaenicke et al (88). Some aspects of Carbonell's work are discussed in Section 3.4, since modifications of the atomic wave function by strong interaction in the annihilation region might generate observable dynamical selection rules in some annihilation channels. This was remarked some time ago by Pilkuhn & Kaufmann (84).

The P-wave energy-level shifts (ΔE) and widths in $\bar{p}$ ^{3}He and $\bar{p}$ ^{4}He atoms have been measured (88a); if ΔE in $\bar{p}$ ^{3}He and the widths of the two isotopes are reproduced in calculations, then ΔE in $\bar{p}$ ^{4}He is about twice that expected from optical potential calculations (89). Only upper limits for the K x rays in $\bar{p}d$ are available (64), and there are conflicting measurement of L x-ray yields (86).

3. ANNIHILATION REACTIONS

There are two main motivations to study low energy annihilation:

1. Since the process involves the annihilation of quark pairs and the emission of gluons (g), $\bar{p}p$ is an excellent source for the production of exotic hadrons like glueballs (gg, ggg, . . .), hybrids ($q\bar{q}g$), and multiquark mesons (for example, $\bar{q}^2q^2$). Recent results regarding these exotic mesons are reviewed in Section 4.
2. The annihilation mechanism itself is not understood. This is nontrivial since annihilation takes place in the nonperturbative regimes of QCD; we must resort to models. Nucleon-antinucleon annihilation at low energy generates an energy density of 1–2 GeV/fm^3, which hadronizes into several mesons. A theoretical effort is now under way to express annihilation into two or three mesons in terms of quark rearrangements

and $\bar{q}q$ annihilations (for a review, see 90) or through the excitation of intermediate meson resonances (32) (see Sections 3.3 and 3.4).

Since annihilation models are currently inspired by data, we first discuss the experimental situation and then review the models that explain some of the relations between the measured branching ratios or cross sections.

3.1 *$\bar{p}p$ Annihilation at Rest*

Earlier data stem from bubble chamber exposures taken in the 1960s at Brookhaven National Laboratory (BNL), Argonne National Laboratory, and CERN (91). In liquid hydrogen, the atomic $\bar{p}p$ S wave dominates annihilation at rest as a result of the Day-Snow-Sucher mechanism (92): following $\bar{p}$ capture in a high n orbital ($n \sim 30$) of the $\bar{p}p$ atom, the $\bar{p}$ is rapidly transferred by collisions with neighboring H_2 molecules to the nS level, where the system annihilates because there is no centrifugal barrier. Hence annihilation with the initial angular momentum $L = 0$ (S-wave annihilation) dominates in liquid hydrogen.

The largest data sample, collected by the CERN–Collège de France collaboration, consisted of 80,000 fully reconstructed pionic events and 20,000 fully reconstructed events with at least one $K_S(\rightarrow \pi^+\pi^-)$. The largest fraction (60%) of all annihilations involving two or more π^0 or η could not be studied in bubble chamber experiments and the early kaonic data suffer from poor statistics. An experimental program has been initiated at LEAR to study annihilation into multineutral and kaonic channels. The Crystal Barrel and Obelix detectors have been commissioned and the first branching ratios from the Crystal Barrel will be published soon.

Recently, two-body branching ratios for π^0M and ηM, where M = π^0, η, η', ϕ, ω, ρ^0, have been determined in liquid hydrogen at KEK (93) and at LEAR (94, 95) by measuring the inclusive η or π^0 momentum spectrum in, for example, $\bar{p}p \rightarrow \pi^0(\eta) +$ anything. These branching ratios are displayed in Table 1, together with earlier measurements for two-body annihilation. The energies and angles of γ pairs were measured by a segmented γ detector. The momentum distribution of the pairs, consistent with π^0 or η decay, shows peaks corresponding to the two-body final states π^0M or ηM. However, since reflections distort the inclusive spectrum in an unpredictable way and the background is often very large, the branching ratios for broad mesons M or for weak annihilation channels cannot be reliably extracted from inclusive spectra. Consequently, exclusive measurements in which all particles are detected must be performed. Strictly speaking, branching ratios can be given only for channels involving narrow

ble 1 Branching ratios BR_{liq} for $\bar{p}p$ annihilation at rest in liquid[a]

hannel	BR_{liq}				Ref.	Channel	BR_{liq}				Ref.
γ	< 1.7			10^{-6}	[94]	$\eta\phi$	< 2.8			10^{-3}	[93]
$^{+}e^{-}$	3.2	±	0.9	10^{-7}	[96]	$\eta'\rho$	1.29	±	0.81	10^{-3}	[100]
$^{0}\gamma$	1.74	±	0.22	10^{-5}	[94]	$\rho^0\rho^0$	1.2	±	1.2	10^{-3}	[91]
$^{0}\pi^{0}$	2.06	±	0.14	10^{-4}	[94]	$\rho\omega$	2.26	±	0.23	10^{-2}	[103]
	4.8	±	1.0	10^{-4}	[97]		3.9	±	0.6	10^{-2}	[104]
	1.4	±	0.3	10^{-4}	[98]	$\omega\omega$	1.4	±	0.6	10^{-2}	[105]
	2.5	±	0.3	10^{-4}	[99]	$\omega\phi$	6.3	±	2.3	10^{-4}	[106]
$^{0}\rho^{0}$	1.72	±	0.27	10^{-2}	[91][b]	$\omega f_2(1270)$	3.26	±	0.33	10^{-2}	[103]
	1.6	±	0.1	10^{-2}	[93]	$\rho f_2(1270)$	1.57	±	0.34	10^{-2}	[91]
$^{0}\omega$	5.2	±	0.5	10^{-3}	[93]	$\pi^{\pm}\rho^{\mp}$	3.44	±	0.54	10^{-2}	[91][b]
$^{0}f_2(1270)$	4.1	±	1.2	10^{-3}	[91]		3.0	±	0.3	10^{-2}	[104]
$^{0}\phi$	3.0	±	1.5	10^{-4}	[93]	$\pi^{+}\pi^{-}$	3.33	±	0.17	10^{-3}	[91]
$^{0}\eta$	3.9	±	1.0	10^{-4}	[93][b]	$K^{+}K^{-}$	10.1	±	0.5	10^{-4}	[91]
	1.33	±	0.27	10^{-4}	[95]	$K^{0}\overline{K^{0}}$	7.6	±	0.4	10^{-4}	[91]
$^{0}\eta'$	5.0	±	1.9	10^{-4}	[93]	$\pi^{\pm}a_0^{\mp}(980)$	6.9	±	1.2	10^{-3}	[104]
η	8.1	±	3.1	10^{-5}	[95]	$\pi^{\pm}b_1^{\mp}(1235)$	7.9	±	1.1	10^{-3}	[103]
	1.6	±	0.8	10^{-3}	[93]		1.96	±	0.27	10^{-2}	[104]
η'	< 1.8			10^{-4}	[95]	$\pi^{\pm}a_2^{\mp}(1320)$	2.83	±	0.32	10^{-2}	[104]
ρ	6.5	±	1.4	10^{-3}	[100]		4.74	±	0.61	10^{-2}	[91][b]
	5.3	±	1.4	10^{-3}	[95]		2.16	±	0.45	10^{-2}	[107, 108][b]
	9.6	±	1.6	10^{-3}	[93]	$K^{0}\overline{K^{0*}}$	1.57	±	0.11	10^{-3}	[91][b]
	5.0	±	1.4	10^{-3}	[101]	$K^{\pm}K^{\mp*}$	1.0	±	0.1	10^{-3}	[91][b]
	2.2	±	1.7	10^{-3}	[102]		1.42	±	0.14	10^{-3}	[104]
ω	1.0	±	0.1	10^{-2}	[95]	$K^{0*}\overline{K^{0*}}$	3.22	±	0.67	10^{-3}	[109]
	4.6	±	1.4	10^{-3}	[93]	$K^{\pm*}K^{\mp*}$	1.54	±	0.54	10^{-3}	[109][b]

The pure S wave BR_S and pure P wave BR_P are related to BR_{liq} by the relation $BR_{liq} = BR_S(1-f_P)+BR_P f_P$, where $\approx 8.6 \pm 1.1\%$ is the fraction of annihilation from atomic P states in liquid hydrogen (110). The branching ratios of the al annihilation rate include the experimentally unobserved decay modes.
[b]Average of two or more measurements.

mesons (π, K, η, η', and possibly ω and ϕ); the branching ratios for broad mesons are not defined because other channels leading to the same final state interfere, even in exclusive measurements. As seen in Table 1, the experimental situation is not satisfactory; many branching ratios are either poorly measured or in conflict with one another. To test the theoretical ideas on annihilation and improve our understanding of these processes, exclusive measurements of few-meson final states are clearly important.

Annihilation from atomic P states has been studied at LEAR by the Asterix collaboration using hydrogen gas at normal temperature and pressure (NTP, meaning here 20°C and 1 atm). In gaseous hydrogen, the molecular collision rate is reduced because of the lower density, the electromagnetic cascade can develop down to the 2P levels, and hence annihilation from atomic P states competes with annihilation from S states. In gaseous hydrogen at NTP, annihilation from all atomic P states occurs with a probability of $52.8 \pm 4.9\%$ (111). Experimental data on S- and P-state contributions were compared with a cascade model calculation by Reifenröther & Klempt (86). Annihilation from D states is expected to be negligible in hydrogen gas at NTP (112). The yield of L x rays (transitions to the 2P levels) is $13 \pm 2\%$ while the yield of K x rays (transitions to the 1S ground state) is $0.65 \pm 0.32\%$ (113). Once in the 2P levels, the $\bar{p}p$ atom annihilates with a probability of $98 \pm 1\%$ and therefore annihilation dominates over the K_α transition (113).

The Asterix group has developed a new technique of preparing the initial state in the atomic 2P states by triggering on the L x-ray transitions to the 2P states (114). A hardware trigger on the initial x-ray candidate typically yields 60–70% P-wave annihilation. The off-line analysis, requiring coincidence with L x rays, then leads to typically 90% P-
residual 10% S-wave annihilation in the signal is due to background contamination from bremsstrahlung x rays under the L x-ray series (115). The bremsstrahlung is produced by the sudden acceleration of charge in the $\bar{p}p$ annihilation final state. The true P-wave contribution, when applying the coincidence with L x rays, depends on the annihilation channel. The exact P-wave fraction in the x-ray coincidence sample depends on the ratio of annihilation branching ratios between S and P states, since bremsstrahlung stems from the annihilation final states not necessarily associated with the emission of an L x ray.

The 105-MeV/*c* antiprotons from LEAR stopped in a NTP gaseous target, which was surrounded by a drift chamber where the x rays of the atomic cascade were converted. Charged particles were reconstructed in a solenoidal magnetic spectrometer and the γ angles were determined by conversion in lead sheets, albeit with a modest efficiency of 25%. Details on the apparatus are described by Ahmad et al (116). By measuring branching ratios in gas (with x-ray enhancing trigger and in off-line coincidence with L x rays) and in liquid, one can determine the branching ratios from pure initial S and P states. The statistics collected by Asterix in gaseous hydrogen exceed the bubble chamber sample by some two orders of magnitude.

3.1.1 ANNIHILATION INTO $\pi^+\pi^-$, K^+K^-, AND $K^0\bar{K}^0$ Figure 5*a* shows the

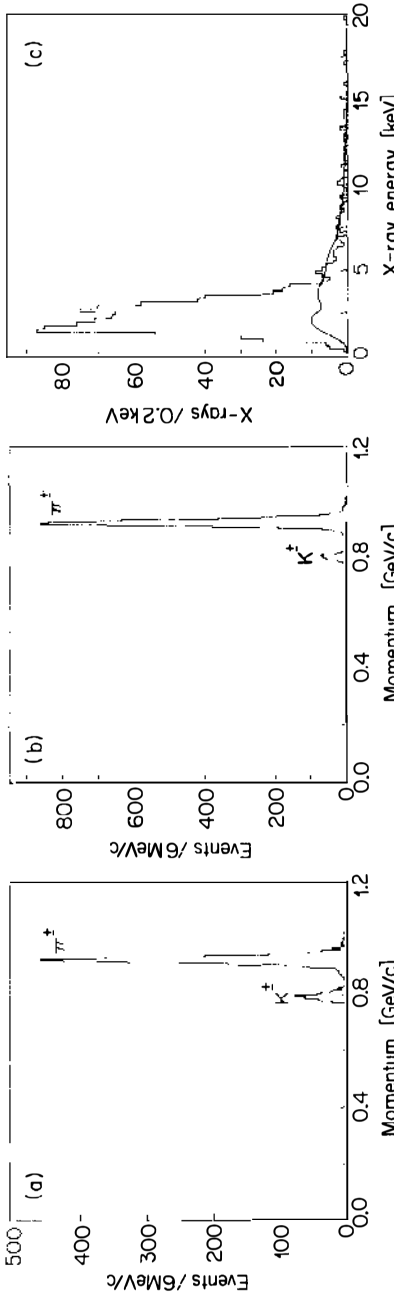

Figure 5 Momentum distribution of collinear events from $\bar{p}p \rightarrow \pi^+\pi^-$ and K^+K^- (*a*) in gas and (*b*) in off-line coincidence with L x rays. (*c*) The x-ray spectrum associated with $\pi^+\pi^-$ events, including the background bremsstrahlung (*solid curve*) (110).

momentum distribution of collinear two-prong events in gaseous hydrogen at NTP (110). The peaks are due to the annihilation channels $\bar{p}p \rightarrow K^+K^-$ and $\pi^+\pi^-$. Figure 5*b* shows the momentum distribution with off-line coincident L x rays. The x-ray spectrum associated with $\pi^+\pi^-$ events is shown in Figure 5*c*. The peak between 1.3 and 4 keV is due to the (unresolved) L x-ray series, the peak around 3.0 keV is due to argon fluorescence in the drift chamber.

A comparison of Figures 5*a* and *b* shows that the K/π ratio decreases with increasing atomic P-wave contribution. The branching ratios for these channels in liquid are given in Table 1, and the pure branching ratios for S and P waves are shown in Table 2. The S-wave annihilation rate in liquid

Table 2 The branching ratios of the total annihilation rate for $\bar{p}p$ S- and P-wave annihilation into the channels measured by the Asterix experiment[a]

	S				P			
K^+K^-	1.08	±	0.05	10^{-3}	2.87	±	0.51	10^{-4}
$K^0\bar{K}^0$	8.3	±	0.5	10^{-4}	8.8	±	2.3	10^{-5}
$\pi^+\pi^-$	3.19	±	0.20	10^{-3}	4.81	±	0.49	10^{-3}
$\rho^\pm\pi^\mp$	3.21	±	0.42	10^{-2}	1.50	±	0.20	10^{-2}
$\rho^0\pi^0$	1.56	±	0.21	10^{-2}	0.40	±	0.09	10^{-2}
$f_2(1270)\pi^0$	3.9	±	1.1	10^{-3}	1.83	±	0.23	10^{-2}
$\pi^+\pi^-\pi^0$	6.6	±	0.8	10^{-2}	4.5	±	0.6	10^{-2}
$\eta\pi^+\pi^-$	1.37	±	0.15	10^{-2}	3.35	±	0.84	10^{-3}
$\eta'\pi^+\pi^-$	3.46	±	0.67	10^{-3}	0.61	±	0.33	10^{-3}
$a_2^\pm(1320)\pi^\mp$	2.69	±	0.60	10^{-2}	9.03	±	4.76	10^{-3}
$\eta\rho$	3.29	±	0.90	10^{-3}	9.4	±	5.3	10^{-4}
$f_2(1270)\eta$	1.5	±	1.5	10^{-4}	1.1	±	0.5	10^{-3}
$\eta'\rho$	1.81	±	0.44	10^{-3}	~ 3			10^{-4}
$\pi^+\pi^-\omega$	6.55	±	0.68	10^{-2}	7.05	±	1.05	10^{-2}
$\rho\omega$	1.91	±	0.37	10^{-2}	6.38	±	1.28	10^{-2}
$\pi^\pm b_1^\mp(1235)$	0.83	±	0.12	10^{-2}	0.67	±	0.18	10^{-2}
$\phi\pi^0$	4.0	±	0.8	10^{-4}	≤ 3			10^{-5}
$\phi\pi^+\pi^-$	4.7	±	1.1	10^{-4}	6.6	±	1.5	10^{-4}
$\phi\rho$	3.4	±	1.0	10^{-4}	3.7	±	0.9	10^{-4}
$\phi\omega$	5.3	±	2.2	10^{-4}	2.9	±	1.4	10^{-4}
$\phi\eta$	3.0	±	3.9	10^{-5}	4.2	±	2.0	10^{-5}

[a] The branching ratios include the unobserved decay modes and the $b_1(1235)$ is assumed to decay exclusively into $\omega\pi$.

hydrogen has been determined by comparing the rates for $\pi^+\pi^-$ from P wave and for $\pi^0\pi^0$ from a liquid target (94). The former, from the P states, should be twice the latter. In fact, neutral pseudoscalar pairs cannot be produced from S waves. This explains the very small branching ratios in liquid. The fraction of P-wave annihilation in liquid into all channels is found to be $8.6 \pm 1.1\%$ (110) when the most precise $\pi^0\pi^0$ datum is used (94). This is the first determination of this important number. As seen in Table 2, the rates strongly depend on the initial angular momentum, with K^+K^- being suppressed by a factor of four when switching from S to P waves, the physics of which is discussed in Section 3.4.

The channel $K^0\bar{K}^0$ appears as K_SK_S from initial P states and as K_SK_L from initial S states. The former has not been observed in earlier bubble chamber experiments. Asterix observed the channels $\bar{p}p \to K_SK_S$ ($K_S \to \pi^+\pi^-$) and K_SK_L ($K_S \to \pi^+\pi^-$, K_L undetected) in hydrogen gas (111). The fraction of P-wave annihilation to all channels in gas was determined (*a*) from the $\pi^+\pi^-$ and K^+K^- branching ratios in gas, liquid, and in off-line coincidence with L x rays, and (*b*) from a comparison of K_SK_L in liquid and gas. The average fraction is $52.8 \pm 4.9\%$ (111), from which one derives the branching ratios for K_SK_S ($K^0\bar{K}^0$ from P waves) given in Table 2. The channel $K^0\bar{K}^0$ is hence suppressed by a factor of 10 when switching from S to P waves.

Since K^+K^- and $K^0\bar{K}^0$ are mixtures of $I = 1$ and $I = 0$ and since the two branching ratios are nearly equal for S states, one deduces that one isospin amplitude dominates, unless the admixtures of $\bar{n}n$ and $\bar{p}p$ are comparable (84, 85, 87, 88), in which case both isospin amplitudes could contribute as discussed by Jaenicke et al (88) (see also Sections 2.3 and 3.4). If one assumes that the $\bar{n}n$ atomic component for this reaction is small and that $\bar{p}n$ annihilates from an S state in deuterium, then one can use the rate for the pure $I = 1$ $\bar{p}n \to K^0K^-$, which is $(1.5 \pm 0.2) \times 10^{-3}$ (117), to find that $I = 1$ $\bar{p}p$ dominates $I = 0$ by a factor of three for annihilation into a $K\bar{K}$ pair (111). However, P waves could contribute significantly in $\bar{p}p$ and $\bar{p}n$ annihilation in deuterium (86), in which case the above argument would not hold. For P states, the much smaller rate for $K^0\bar{K}^0$ indicates that both isospins contribute from initial P states, contrary to theoretical expectations (84) (see Section 3.4).

3.1.2 ANNIHILATION INTO $\pi^+\pi^-\pi^0$ This annihilation channel was studied earlier in bubble chambers, where S-wave annihilation dominates (118). The salient feature is a dominating $\rho\pi$ channel produced mainly from the ($I = 0$) $^3S_1$ initial state and strongly suppressed from the ($I = 1$) $^1S_0$ state. This is sometimes referred to as the $\rho\pi$ puzzle (Section 3.4).

Asterix has analyzed the $\pi^+\pi^-\pi^0$ channel in gaseous hydrogen and in

off-line coincidence with L x rays (meaning $91.8 \pm 1.0\%$ P wave) (119). Including data in liquid (118) one finds the pure $\bar{p}p$ S- and P-wave branching ratios given in Table 2. The Dalitz plot and the projections are shown in Figure 6. One notices a strong production of $f_2(1270)$ and a peak at 1565 MeV ascribed to a new resonance, $f_2(1565)$, discussed in Section 4.2.2. The state $f_2(1270)$ is only weakly produced in liquid and $f_2(1565)$ is not observed (118). A close examination of Figure 6 shows that $f_2(1270)$ and $f_2(1565)$ productions increase with increasing P-wave probability (Figure 6*c* vs Figure 6*d*), while the ratio of ρ^0 to $\rho^\pm$ decreases. This indicates that the $I = 1$ contribution (from which state the reaction $\bar{p}p \to \rho^0\pi^0$ is forbidden) increases with increasing P wave, provided that the relative ratio of $\bar{n}n$ to $\bar{p}p$ remains very small and roughly the same for this reaction in both atomic S and P states.

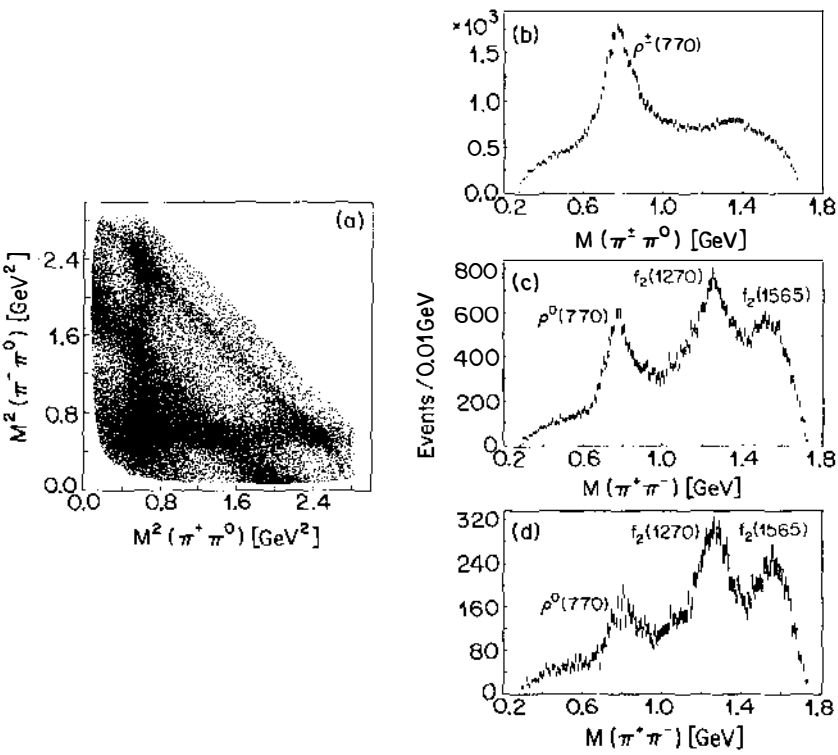

Figure 6 (*a*) Dalitz plot for the channel $\bar{p}p \to \pi^+\pi^-\pi^0$ in gas; (*b*) $\pi^\pm\pi^0$ invariant mass distribution; (*c*) $\pi^+\pi^-$ invariant mass distribution; (*d*) $\pi^+\pi^-$ invariant mass distribution requiring off-line coincidences with L x rays (119).

Table 3 Two-body and direct 3π contributions to $\pi^+\pi^-\pi^0$ for $\bar{p}p$ annihilation from S and P waves as a percentage of the total annihilation rate (119)

	$^3S_1$	$^1S_0$	$^1P_1$	$^3P_1$	$^3P_2$
$\rho^\pm\pi^\mp$	3.12 ± 0.42	0.09 ± 0.04	0.80 ± 0.17	0.67 ± 0.11	0.03 ± 0.01
$\rho^0\pi^0$	1.56 ± 0.21		0.40 ± 0.09		
$f_2(1270)\pi^0$		0.22 ± 0.06		0.95 ± 0.13	0.09 ± 0.03
$f_2(1565)\pi^0$				0.24 ± 0.04	0.14 ± 0.03
Direct 3π[a]	1.61 ± 0.03			1.18 ± 0.05	

[a] The direct 3π contributions refer to the total S- or total P-wave rates.

A Dalitz plot analysis in terms of pure S waves has been performed by subtracting the Dalitz plot corresponding to Figure 6*d* (off-line coincidence with L x rays) with a floating normalization from the Dalitz plot of Figure 6*a* (annihilation in gas), thereby subtracting the P-wave contribution, and fitting all contributing amplitudes from the $^3S_1$ and $^1S_0$ initial states. The fit agrees perfectly with the results from the bubble chamber experiment (118), which indicates that corrections for detector acceptance have been applied properly. An analysis of the P-wave Dalitz plot has then been performed. Table 3 summarizes the branching ratios for all contributions to $\pi^+\pi^-\pi^0$. Note that the values in Table 3 are calculated from the amplitudes by adding all amplitudes incoherently, thereby neglecting interference effects.

3.1.3 ANNIHILATION INTO $\eta\pi^+\pi^-$, $\eta'\pi^+\pi^-$, AND $2\pi^+2\pi^-\pi^0$ Asterix has studied the channel $\bar{p}p \to \eta\pi^+\pi^-$ where (*a*) $\eta \to \pi^+\pi^-\gamma$ or (*b*) $\eta \to \pi^+\pi^-\pi^0$ and the channel $\bar{p}p \to \eta'\pi^+\pi^-$ where (*c*) $\eta' \to \pi^+\pi^-\gamma$ or (*d*) $\eta' \to \pi^+\pi^-\eta$. For reactions (*b*) and (*d*) the π^0 and η were kinematically reconstructed, while for reactions (*a*) and (*c*) the photon was detected by conversion in the lead sheets. These four-prong events were collected with the x-ray enhancing trigger (meaning 61% P wave) and in off-line L x-ray coincidence (meaning 86% P wave) (120). Figure 7*a* shows the $\pi^+\pi^-\pi^0$ invariant mass distribution for the final-state $2\pi^+2\pi^-\pi^0$ and 61% P wave. Figure 7*b* shows the $\pi^+\pi^-\gamma$ spectrum in the four-prong channel for 61% P wave. The background from $2\pi^+2\pi^-\pi^0$ with one γ escaping detection has been subtracted. An upper limit of 3×10^{-3} for $\omega \to \pi^+\pi^-\gamma$ is obtained by comparing ω production in $2\pi^+2\pi^-\pi^0$ and $2\pi^+2\pi^-\gamma$. This is an order-of-magnitude improvement on the upper limit for this decay. Figure 7*c* shows the $\eta\pi^+\pi^-$ spectrum in the η' region.

The branching ratios for the two reactions $\eta\pi^+\pi^-$ and $\eta'\pi^+\pi^-$ have been determined using the known η and η' decay branching ratios and averaging the results from reactions (*a*) and (*b*) with (*c*) and (*d*), respectively. These

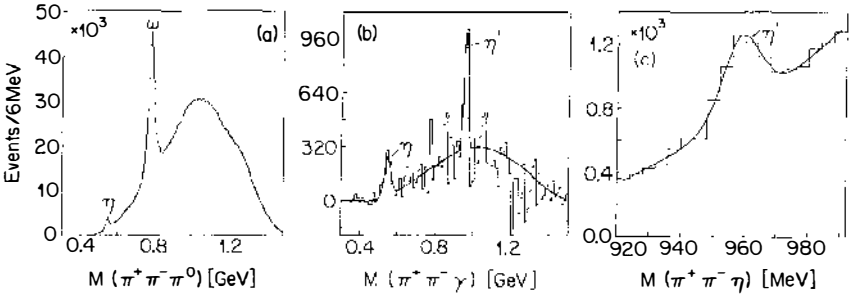

Figure 7 Invariant mass distritubtions for (*a*) $\pi^+\pi^-\pi^0$, (*b*) $\pi^+\pi^-\gamma$, and (*c*) $\pi^+\pi^-\eta$ for four-prong annihilation events (120).

branching ratios have also been measured in liquid (100, 101). The results for pure S and P waves are given in Table 2. Both branching ratios decrease with increasing P wave, typically by a factor of five when switching from S to P waves.

A fraction of $51 \pm 10\%$ of the $\eta'\pi^+\pi^-$ final state proceeds through the $\eta'\rho$ final state in liquid (100). This agrees with Asterix data for S states (although no Dalitz plot analysis has been performed because of the low statistics) and also for P states within the large statistical errors. A Dalitz plot analysis has been applied to the final-state $\eta\pi^+\pi^-$ with the decay $\eta \to \pi^+\pi^-\pi^0$ (reaction *b*). Initial S- and P-wave contributions were derived by subtracting the 86% P-wave Dalitz plot from the 61% P-wave Dalitz plot, as described in the previous section for the three-pion final state. The branching ratios for the intermediate states $a_2^{\pm}(1320)\pi^{\mp}$, $f_2(1270)\eta$, and $\eta\rho$ (corrected for the unobserved decay modes) are given in Table 2. One notes, as for the three-pion final state, a large enhancement of $f_2(1270)$ production when switching from S to P waves. A 2σ effect of $(1.3 \pm 0.7) \times 10^{-4}$ for the annihilation channel $\bar{p}p \to a_0^{\pm}(980)\pi^{\mp}$, with $a_0^{\pm}(980) \to \eta\pi^{\pm}$, is also observed.

The ratio of $\eta\rho$ to $\eta'\rho$ equals 2.5 ± 0.7 and thus is compatible with a larger $s\bar{s}$ component in the η', a component that does not contribute strongly to annihilation because of the Okubo-Zweig-Iizuka (OZI) rule. Ignoring phase-space differences, one naively expects a ratio of two, if one assumes a pseudoscalar mixing angle of $-20°$ and uses the standard SU(3) flavor meson wave functions of the simple constituent quark model (120). However, care should be taken when using these simple arguments: the ratio of $\pi^0\eta$ to $\pi^0\eta'$ is about one according to the branching ratios in Table 1, but is expected to be two. These ratios should be measured more precisely to test this simple model.

The Asterix collaboration has also derived branching ratios for the

channels $\pi^+\pi^-\omega$, $\rho\omega$, and $b_1(1235)^{\pm}\pi^{\mp}$ for both S and P states (121), starting from the same four-prong data samples as in the previous section, but selecting events associated with ω production (see Figure 7*a*). The results are given in Table 2. The channel $\rho\omega$ proceeds from the spin-singlet S state or from the three spin-triplet P states. This may explain the strong enhancement of $\rho\omega$ production from P states.

3.1.4 ϕ PRODUCTION IN $\bar{p}p$ ANNIHILATION AT REST AND THE OZI RULE It has been suggested that an enhanced production of ϕ mesons could be related to an excess of $s\bar{s}$ pairs in the nucleon (122) or to flavor mixing (123–125) with a $\bar{q}^2q^2$ state below threshold containing an $\bar{s}s$ pair. Such a state C(1480) ($\rightarrow \phi\pi^0$) was recently reported at Serpukhov (126). If the nucleon and antinucleon do not contain any strange quarks, ϕ production should be suppressed in $\bar{p}p$ annihilation by the OZI rule. A naive estimate of the ratio R of the ϕ to ω rates is given by the deviation from ideal mixing in the vector meson nonet. Neglecting phase-space factors, one expects a value

$$R = \mathrm{BR}(\phi)/\mathrm{BR}(\omega) = \tan^2(\Phi - \Phi_i) = 4.2 \times 10^{-3}, \qquad 4.$$

where Φ_i is the ideal mixing angle of 35.3° and $\Phi = 39°$, when the quadratic mass formula is used. (An even smaller ratio occurs with the angle of $\Phi = 36°$ from the linear mass formula.)

The Asterix collaboration has analyzed the final states $\phi\pi^0$, $\phi\pi^+\pi^-$, $\phi\rho^0$, $\phi\eta$, and $\phi\omega$, where the ϕ is observed in its K^+K^- decay mode and the ω and η in their $\pi^+\pi^-\pi^0$ decay modes, from initial states with 61% P wave and with 86% P wave for four-prong events (59 and 93% P wave for two-prong events, respectively) (127). The charged kaons were identified by ionization sampling. The channel $\pi^0\phi$ and its $\pi^0\omega$ counterpart have been observed in liquid hydrogen from a study of the inclusive π^0 spectrum (93). Together with the Asterix data, one obtains the pure S- and P-wave branching ratios for $\phi\pi^0$ shown in Table 2. Ignoring phase-space differences, one finds $R = (7.7 \pm 1.7) \times 10^{-2}$ from the $\bar{N}N\ ^3S_1$ wave, an order of magnitude larger than the naive estimate of Equation 4.

For $\phi\pi^+\pi^-$ and $\phi\rho$ ($\rho \rightarrow \pi^+\pi^-$) the contributions from S and P waves are fitted for both the 61% and the 86% P-wave data samples (127). The branching ratios for pure S and P waves are given in Table 2. The S-wave branching ratio for $\phi\pi^+\pi^-$ agrees with an earlier measurement in liquid hydrogen (103). From the values shown in Table 2, one then finds for $\phi\pi^+\pi^-$ and $\omega\pi^+\pi^-$ $R = (7.1 \pm 1.8) \times 10^{-3}$ for S waves and $R = (9.4 \pm 2.5) \times 10^{-3}$ for P waves. Similarly for $\phi\rho$ and $\omega\rho$ one gets $R = (1.8 \pm 0.6) \times 10^{-2}$ for $^1S_0$ and $R = (5.8 \pm 1.8) \times 10^{-3}$ for P waves.

The branching ratios for $\phi\omega$ for pure S and P waves can again be

calculated using the branching ratios in liquid (106) (Table 1). Taking the branching ratio for $\omega\omega$ in liquid (105) one finds $R = (3.8 \pm 2.2) \times 10^{-2}$ for $^1S_0$. For $\phi\eta$ one obtains together with the branching ratio for $\omega\eta$ in liquid $R = (2.9 \pm 3.8) \times 10^{-3}$. A test of OZI violation for $\phi\eta$ and $\phi\omega$ from P waves is not possible since the branching ratios for $\omega\eta$ and $\omega\omega$ are not known from P waves.

To discuss a possible OZI violation, one should correct for phase-space differences, which are largest when ϕ is slow. However, the phase-space correction is unclear. For large momenta p in the final state, the correction is simply p. For low momenta the phase-space factor following Blatt and Weisskopf is proportional to $p[p^2/(p^2+\mu^2)]^l$, where μ is the inverse range of the interaction (including any finite size of the particles) and l is the relative two-meson angular momentum. This certainly is the case for $\phi\rho$ ($\lambda = 4.5$ fm $\gg 0.2$ fm) and hence the ratio $\phi\rho/\omega\rho$ would increase by a factor of two. On the other hand, Vandermeulen's phase-space factor does not modify the ratio R significantly (123) (see also Section 3.4). Given the large experimental uncertainties, the size of the OZI violations in some branching ratios is sensitive to the theoretical prescription for the phase-space contribution used in each case.

The evidence for OZI rule violation is hence weak, except for the channel $\phi\pi^0$ compared to $\omega\pi^0$, for which the phase-space factors are similar (and possibly for $\phi\rho$ from the $^1S_0$). A strong violation has also been observed in liquid deuterium: from the average of three measurements for $\bar{p}n \to \pi^-\phi$ (108, 128, 129) and of three measurements for $\bar{p}n \to \pi^-\omega$ (130–132), one finds a very large value, $R = 0.14 \pm 0.02$. It should also be noted that, at higher energies, ϕ production seems enhanced in both pp and $\bar{p}p$ interactions (133).

3.1.5 EXPERIMENTAL STATUS OF NARROW $\bar{N}N$ BOUND STATES As discussed in Section 2.1.3, baryonium states could arise from the strongly attractive meson exchange potential. Narrow baryonia have been sought by searching for narrow lines in the γ, π^0, and $\pi^\pm$ inclusive spectra of $\bar{p}p$ annihilation at rest. The earlier evidence for narrow states associated with monochromatic γ emission (134) has neither been confirmed at KEK (135) nor at LEAR (136, 137). The 95% confidence level upper limit for the production of states narrower than 25 MeV is 8×10^{-5} of all annihilations for a mass of 1100 MeV, rising to 5×10^{-4} for a mass of 1780 MeV (for a review, see 18, 138). For monochromatic $\pi^\pm$ emission, the experimental limit is typically 4×10^{-4} (139) and for π^0 monochromatic emission, typically 2×10^{-3} (99).

Asterix has also looked for states associated with the emission of a $\pi^\pm$

from initial atomic P states, since narrow states were predicted to have a high angular momentum and might hence be enhanced from P states. No narrow state was found in the mass range 1100 to 1670 MeV with a 95% confidence level upper limit of 7×10^{-4} (138, 140).

The experimental evidence pertains to the existence of narrow states ($\Gamma \leq 25$ MeV). Broad states cannot be observed from inclusive spectra and are therefore not excluded. In Sections 4.2.2 to 4.2.4 on spectroscopy, we discuss the evidence for the broad (~ 170 MeV) $f_2(1565)$ proposed to be a deeply bound 2^{++} ($I = 0$) baryonium (141). Finally, we point out that narrow states very close to the $\bar{N}N$ threshold, which could be produced by the emission of soft photons (≤ 100 MeV), are not excluded.

3.2 *$\bar{p}p$ Annihilation in Flight*

Little progress has been made in the recent years in studying $\bar{p}p$ annihilation into exclusive final states above the $\bar{N}N$ threshold. The angular distribution for the two-body final states $\pi^-\pi^+$ and K^-K^+ has been studied by KEK between 360 and 760 MeV/c (142). This experiment did not determine the charges of the emitted mesons and hence could not distinguish between forward and backward scattering. The angular distributions for $\pi^-\pi^+$ and K^-K^+ show a peak for $|\cos\theta|$ close to unity.

An earlier experiment at KEK, which measured the full (unfolded) angular distribution, reported a strong forward peak for $\pi^-\pi^+$ and strong peaks in both forward and backward directions for K^-K^+ (143). The backward peak in K^-K^+ was also observed earlier at 790 MeV/c (144). However, the energy dependence of the integrated cross sections for the new KEK experiment (142) is at variance with the old KEK experiment (143) and in particular does not confirm the strong enhancement seen in the K^-K^+ channel around 500 MeV/c. Hence the existence of a backward peak in K^-K^+ at very low energy needs to be clarified. Data for these reactions have been collected at LEAR between 360 and 1550 MeV/c in connection with a measurement of the analyzing power (145), but results are not available yet. A second experiment at LEAR has measured the angular distributions below 300 MeV/c (146). The $\pi^-\pi^+$ angular distribution is very strongly asymmetric, even at very low momentum (225 MeV/c), rising quickly in the forward hemisphere, while K^-K^+ remains flat. However, the angular coverage of this second experiment does not extend to small enough forward nor large enough backward scattering angles to clarify the earlier KEK experimental results. A backward K^-K^+ peak cannot be reproduced by any quark model (60) nor by a simple baryon exchange model (147–149) but a backward peak is found in the coupled-channel calculation of Liu & Tabakin (39). However, this latter work found some deep minima not observed in the $\pi^-\pi^+$ differential cross

section. This backward peak could signal the formation of an s-channel resonance or, as has also been speculated, it could be due to the exchange of a strangeness +1 exotic baryon in the t channel, enhanced by the admixture of strangeness in the proton (122).

The integrated cross section for $\pi^-\pi^+$ rises very quickly with decreasing $\bar{p}$ momentum, while K^-K^+ seems to be constant from about 800 down to 200 MeV/c (142, 146, 150), a trend that is reproduced by quark models (149, 151).

Data for the analyzing power in $\pi^-\pi^+$ and K^-K^+ are now available from LEAR between 360 and 1550 MeV/c (145). The analyzing power is very large for broad regions of the angular range, even reaching the maximum value of one. This latter means that the π^- or K^- are always scattered to the left of the beam for a target proton 100% polarized along the normal to the scattering plane. This remarkable behavior is not understood (37).

The annihilation into an e^-e^+ pair has also been studied at LEAR between 416 and 888 MeV/c in order to determine the form factor of the proton in the timelike region (152). The isotropic angular distribution at low momentum is consistent with the electric and magnetic form factors being equal. More surprisingly, the dependence of the form factor on the incident $\bar{p}$ energy is steeper than predicted by the vector dominance model and furthermore seems to oscillate. This latter behavior leads to speculations about the existence of $\bar{N}N$ resonances or bound states close to $\bar{N}N$ threshold (153). However, these states should also be seen in the $\bar{p}d \rightarrow p5\pi$ data, since these latter reactions probe the $\bar{N}N$ amplitude above and below threshold, as discussd by Fasano & Locher (66).

3.3 *Models for the Global Annihilation Process*

On the average, $\bar{N}N$ annihilates into five pions at low $\bar{p}$ energies, although $\bar{p}p$ at rest can in principle decay into $13\pi^0$. For a given number of pions, the charge is distributed statistically according to the model of Pais (30) discussed in Section 2.1.2. This statistical notion of the bulk properties of annihilation is corroborated by the hot gas model, which describes the energy spectrum of charged pions emitted in the annihilation reaction $\bar{p}p \rightarrow$ hot gas $\rightarrow \pi +$ anything (29). It is assumed that $\bar{N}N$ annihilates into fragments that are in thermal (or nearly thermal) equilibrium and that the pions evaporated from this hot gas have the same energy distribution as the fragments. Following Kimura & Saito (29) and others, the cross section is

$$d^3\sigma/dk^3 \propto k^2 \exp(-\omega/T), \qquad 5.$$

where $\omega = (m_\pi^2 + k^2)^{1/2}$ is the pion energy and the factor k^2 is required by

Adler's soft pion consistency condition. The temperature T is determined from the measured cross section and found to be ~ 100 MeV (29). This type of model should be developed further for $\bar{p}p$ annihilation, since the arguments are analogous to the ones used in relativistic heavy-ion physics to search for the quark-gluon plasma. In fact, $\bar{p}p$ annihilation is a small-scale laboratory for concepts used in describing the quark-gluon plasma.

Another successful model, which describes the bulk properties of annihilation, is the threshold dominance model (154), discussed by Vandermeulen (32). He assumes that $\bar{N}N$ annihilation proceeds via two-meson intermediate doorway states and that the intermediate two-meson thresholds closest to the actual $\bar{N}N$ total energy dominate (see Equation 6 below). The reaction is $\bar{N}N \rightarrow a + b \rightarrow$ final-state pions (and kaons). Here a and b are all possible pairs of intermediate S- and P-wave $\bar{q}q$ mesons that decay (with known branching ratios) into the specific final state under consideration. Vandermeulen further assumes that the different intermediate two-meson channels leading to the same final state add incoherently. The branching ratio for the production of a pair of nonstrange mesons a and b is parametrized for $E_{\text{c.m.}} > m_a + m_b$ as

$$\text{BR} = pC_{ab} \exp\{-A[E^2_{\text{c.m.}} - (m_a + m_b)^2]^{1/2}\}, \qquad 6.$$

which when multiplied by the measured total annihilation cross section gives the cross section for each annihilation channel. The factor p is the two-meson cms momentum and the coefficient C_{ab} is the average weight of the spin and isospin factors for the reaction. The threshold parameter $A = 1.2\ \text{GeV}^{-1}$ is determined from a fit to the total cross section for $\bar{p}p \rightarrow \pi^-\pi^+$ as a function of energy. This model reproduces the increasing value of the average multiplicity $\langle n \rangle$ with increasing $\bar{p}$ energy (32). Its success is impressive. It also reproduces the various $\bar{p}p$ cross sections into the different charge combinations of two and up to eight pions in the final state, from threshold and up to $p_{\text{lab}} \simeq 3.5$ GeV/c (32). Again, as in the model of Pais, it is the statistical distribution of the charges for each value of n that is partly responsible for this success.

Equation 6 is multiplied by a factor 0.15 to describe the suppression of strange final states ($\bar{K}K$ plus pions). This factor is determined from the total amount of K production and is sufficient to reproduce correctly the cross sections for the final states $\bar{K}K$ with one and up to five pions. Only the experimental cross section for $\bar{p}p \rightarrow K^-K^+$ turns out to be larger than what this simple model predicts. A suppression of strange final states is expected, according to Dosch & Gromes (155), who studied $\bar{q}q$ creation in a background chromoelectric field similar to Schwinger's e^+e^- creation in an electric field. As pointed out by Dover & Fishbane (123), the suppression of strange annihilation channels does not permit a large $\bar{s}s$ ad-

mixture in the nucleon (or antinucleon), in contrast to the claim of Ellis et al (122). Further efforts along Vandermeulen's line of thought, such as the work of Mundigl and collaborators (149), is called for, as we discuss in the next section in connection with specific meson final states. However, an understanding of the crucial two-meson threshold dominance mechanism in this model is necessary.

These three models, especially the last one, give clues as to what is required for describing annihilation through coupled-channel calculations (CCC) in baryon exchange models (39, 69). Accordingly, the lightest mesons are not too important in CCC to account for the major part of the annihilation. They are suppressed by meson-baryon vertex factors or by the threshold factor of Equation 6. Instead, heavier doorway pairs of mesons should be included with increasing $\bar{N}N$ energy. Threshold dominance arises naturally in the baryon exchange model, where the dominant pairs of meson channels are the ones with minimum energy and momentum transfer at the two meson-baryon vertices. The baryon exchange models (37, 39, 40, 47, 147) should therefore be developed further to enhance our understanding of Vandermeulen's results.

3.4 *Annihilation to Specific Meson States*

For annihilation in flight, many initial $\bar{p}p$ waves are involved and the assumption of statistical distribution of quantum numbers should be reasonable. A doorway model with two-meson intermediate states in the s channel, similar to the threshold dominance model (32), is used in several DWBA calculations (37, 47, 147). In a CCC, Liu & Tabakin introduce four effective (fictitious) channels (in addition to the $\pi\pi$ and $\bar{K}K$ channels) to simulate annihilation, and they calculate the differential cross sections for $\bar{p}p \to \pi^-\pi^+$ and K^-K^+, as well as the differential cross sections for elastic and charge exchange scattering (39). As mentioned in Section 3.2, Liu & Tabakin and others (60, 147, 151) have problems reproducing the measured differential cross sections of Tanimori et al (143).

At rest, annihilation occurs from well-defined $\bar{N}N$ states (S and P waves) and Vandermeulen's model has very limited success (32). One main experimental result is that the branching ratio for $\bar{p}p \to \pi^+\pi^-$ is roughly the same from atomic S and P states, whereas the reaction $\bar{p}p \to K^+K^-$ is suppressed from initial P states relative to S states by a factor of about four (110) (see Table 2). The Aarhus group presented a very thorough model-independent analysis of $\bar{p}p$ annihilating into two pseudoscalar mesons (156). When applying this analysis to $\bar{p}p \to K^+K^-$, using the transition matrix $\bar{N}N \to \bar{K}K$ from the quark model of Kohno & Weise (KW) (60), they derive a branching ratio from atomic S states of $\sim 2 \times 10^{-3}$, twice the measured value, but find a branching ratio of

2.2×10^{-4} from P states, in rough agreement with data; hence $\bar{K}K$ is suppressed by one order of magnitude when going from atomic S to P states. For the $\pi^+\pi^-$ final state the Aarhus group, using the quark model of KW, finds that their calculated branching ratio from the atomic S state agrees with LEAR data, but that from the spin-averaged atomic P state is too large by a factor of 40. However, the helicity amplitudes for $\bar{N}N \rightarrow \pi\pi$ scattering calculated by Martin & Morgan (157) (who used crossing symmetry and dispersion relations) fit the $\pi^+\pi^-$ branching ratio from both S and P states within a factor of two (156). The Aarhus group points out that the $\pi^+\pi^-$ rate from the atomic $^3P_0$ state is too large in the KW model and causes the large discrepancy with data. This work is recommended reading for researchers in this field (87, 156). Further model-dependent discussions regarding the rate of $\bar{K}K$ from P and S states are given by Furui et al (158). They use the $^3P_0$ quark annihilation model, which has some success describing meson decays, and explain the rate by arguing that one particular quark diagram dominates the annihilation process.

There are two major weak points in these discussions. The branching ratio for annihilation from a particular atomic state is strongly affected both by the atomic state wave function, which is distorted by strong interaction for $\bar{N}N$ distances less than 2 fm, and by the effective operator describing the transition of $\bar{N}N$ to mesons. Carbonell et al, in a highly recommended paper, used the atomic wave function (distorted by a MEP model) with effective transition operators from a quark model to calculate branching ratios into various two-meson final states (85). However, they have only limited success when comparing with experimental branching ratios. In the spirit of the works of Povh & Walcher (159) and Shibata (46), they plot the calculated annihilation densities as a function of $\bar{N}N$ separation distance for the various initial atomic states. They and other groups find that the spatial region of maximal annihilation density varies with the atomic state and extends from 0.5 to 1.2 fm (47, 160). The precise region depends on the MEP model.

The long-range MEP has coherent tensor forces from the different meson exchanges, as discussed by Dover & Richard (161). For coupled partial waves like $^3S_1$ and $^3D_1$, the overall D-wave probability in the atomic S state is tiny, but for $r < 1$ fm the S and D waves are equally important in some annihilation channels (see Figure 1e of Ref. 85). The importance of the D wave was exploited by Maruyama, who used a particular MEP model and a quark model transition matrix to explain the $\rho\pi$ puzzle (162) (Section 3.1.2). However, Mundigl et al, using a MEP model different from Maryuama and postulating an effective $\bar{N}N$ to two-meson transition potential, did not resolve the $\rho\pi$ puzzle (160). One weak point of these calculations is the arbitrary short-range parametrizations of the MEP for

$\bar{N}N$ distances shorter than 1 fm (12). The strength of the tensor potential at short distances is very uncertain and can strongly affect the calculated branching ratio, therefore easily changing the conclusions (12, 40, 160). For the same reason, the strong tensor force used by Carbonell et al has been criticized by the Aarhus group in their model-independent helicity amplitude analysis of protonium annihilation into two mesons (87). The $\rho\pi$ puzzle remains unsolved.

The short-distance uncertainty of the MEPs also affects the isospin mixing in the short-distance atomic wave function. This mixing is very sensitive to which MEP (Bonn or Paris) model is employed (163). The initial-state isospin mixing strongly affects the calculated neutral and charged $\bar{K}K$ and $\overline{K^*}K$ branching ratios (see also 158, 160). Because of the short-distance theoretical uncertainty ($r < 1$ fm), an analysis to determine the isospin mixture of the various $\bar{N}N$ initial states, like the one of Klempt (164), should be pursued.

A surprising result is found by Mundigl et al when they reproduce the shape of the $\pi^+\pi^-$ mass spectrum in the $\pi^+\pi^-\pi^0$ final state from atomic P states, using Vandermeulen's model, and also find the relative rate of the ρ to $f_2(1270)$ peaks (165). No interference or rescattering of the final mesons are included in this calculation. However, the experimental results in Table 3 for P-wave annihilation into $\pi^+\pi^-\pi^0$ indicate that 27% of the rate proceeds through the direct emission of three pions. The two-meson doorway assumption ignores this direct three-pion contribution and therefore cannot reproduce the overall measured rate correctly.

As discussed, the initial-state interaction and the effective transition matrices for $\bar{N}N$ into mesons are both very important to calculate the meson branching ratios from $\bar{p}p$ at rest. Since the overlap of the quark cores allows annihilation to take place, it is natural to resort to quark models to calculate these transition matrices. These quark model calculations were reviewed by Green & Niskanen (90). They employ many parameters and various arguments to neglect one type of quark diagram and not others. (For recent quark model calculations, see 163, 166–170.)

At this time, it is not clear what we have learned from these quark model calculations or which measured branching ratios are sensitive to explicit quark dynamics. Part of the problem is that there still are conflicting measurements of branching ratios; furthermore we do not yet have an agreed set of reasonable model approximations for the quark-gluon dynamics in the nonperturbative region of QCD. Regarding the quark diagram calculations, a word of caution comes from the work of Green et al (171), reiterated by Carbonell et al (85). The size of the final mesons can influence markedly the annihilation rate, whereas the size of the nucleon

just determines the spatial interaction volume. In fact, some quark diagrams do not contribute if the final two mesons are pointlike. To investigate the various effective transition operators, both effective meson-baryon models and quark models should be used. One hopes a consensus will emerge as to which approximations are viable and whether or not we are seeing signs of the underlying quark dynamics.

A minimalist approach based on the quark line rule (QLR) is taken by Genz et al (166) and Hartmann et al (167), who argue that only the flavor flow in the different quark diagrams is relevant (the effective transition operators being unity and the initial-state interactions being neglected). An example of a QLR argument is the OZI rule, which is applied to ϕ-meson final states in Section 3.1.4. Another example of the QLR is the following: the QLR does not allow (*a*) the final-state configuration $(\bar{u}u)(\bar{d}d)$ if two $\bar{q}q$ pairs annihilate and a new pair is created (annihilation or planar graph) or (*b*) the configuration $(\bar{d}d)(\bar{d}d)$ if only one pair annihilates while the other two pairs are reshuffled (rearrangement graph) (166). The ratios of branching ratios will depend on whether annihilation or rearrangement dominates the annihilation process. For instance, the branching ratios for $\rho^0\rho^0$ and $\omega\omega$ are equal if the annihilation graph dominates. This does not appear to be true experimentally (Table 1). To really test the QLR in $\bar{N}N$ annihilation, the branching ratios for the neutral two- and three-meson final states have to be measured with the Crystal Barrel detector at LEAR.

One topic warrants further study: Is the argument of Richards and coworkers (85, 172) correct that the various annihilation reactions take place at different $\bar{N}N$ distances? These authors make the analogy with muonium (μ^+e^-)-antimuonium (μ^-e^+) annihilation. In this pure QED process, the complete annihilation reaction, with only photons in the final state, takes place at very short distances on the atomic scale. On the other hand, the rearrangement process giving $\mu^+\mu^- + e^+e^-$ in the final state is governed by the spatial overlap of the initial- and final-state wave functions. Richard et al apply these arguments to $\bar{N}N$ annihilations (85, 172) and state that the reaction $\bar{N}N \to \phi\phi$, in which all initial $\bar{q}q$ pairs are annihilated, presumably occurs at a much shorter $\bar{N}N$ separation than, for example, the reaction $\bar{N}N \to 3\pi$, which can be generated by rearrangement of the three initial $\bar{q}q$ pairs (no $\bar{q}q$ annihilations) (172). The latter reaction may occur when the N and $\bar{N}$ quark cores overlap.

In summary, we only have a rudimentary model-dependent understanding of the measured two-meson annihilation branching ratios. One reason is the large inherent short-distance uncertainties of the meson exchange potential. Another open question is which effective transition operators should be used to mimic the annihilation dynamics. With the

forthcoming results from LEAR, we are at least able to resolve a few well-defined questions: (*a*) Is $\rho\rho$ really so weak compared to $\rho\omega$ or $\omega\omega$? (*b*) What is the origin of the $\rho\pi$ puzzle? Do other final states exhibit similar behavior? (*c*) What is behind the suppression or enhancement of various annihilation channels, like $\bar{K}K$, when switching from atomic S to atomic P states? (*d*) Why is the ratio $BR(\phi\pi)/BR(\omega\pi)$ so large compared to the ratio $BR(\phi\pi\pi)/BR(\omega\pi\pi)$? Is this due to an exotic meson $(\bar{q}^2q^2) = C(1480)$? Can we use the observed global suppression of strangeness in the final states to argue against a large $\bar{s}s$ component in the nucleon? As always in strong interaction physics, progress is slow, but with the new data we are increasing our understanding of some aspects of the annihilation reactions.

4. MESON SPECTROSCOPY

4.1 *Overview*

In the past, $\bar{p}p$ annihilation has been a rather successful tool to investigate the spectrum of light quark mesons. The E meson, now $\eta(1440)$, and the $K_1(1270)$ were discovered in $\bar{p}p$ annihilation at rest (173, 174), while the ω and $f_1(1285)$ were first observed in annihilation in flight (175, 176). These experiments were performed in the 1960s in bubble chambers.

At LEAR, a large statistical sample of $\bar{p}p$ annihilation at rest in hydrogen gas has been collected by the Asterix collaboration. These studies mainly pertain to annihilation from atomic P states. Quantum number conservation restricts the possible final-state configurations, and hence the rates for the production of meson resonances are different from S and P states. For example, the production of two identical neutral pseudoscalar mesons is forbidden from S states but allowed from P states, and is thus suppressed in liquid hydrogen. Furthermore, the production of neutral $J^{PC} = 1^{++}$ mesons (for example, $\bar{p}p \rightarrow \pi^0 f_1$) is forbidden from S states for the same reason, while $\pi\pi f_1$ is phase-space suppressed from S states. Hence the production of $f_1(1285)$ and $f_1(1420)$ is suppressed in bubble chamber experiments (see also Section 4.2.1). Annihilation from P states might therefore reveal new states. Asterix has already found, apart from a strong signal for $f_2(1270)$ production from P states, a new state $f_2(1565)$ in the three-pion final state (discussed below).

Antiproton annihilation at rest in gas can be performed only at LEAR because only the cooled low energy beams have the necessary small-range straggling and narrow momentum spread. Furthermore, with the advent of new technologies like CsI scintillators read out by photodiodes in strong magnetic fields, large solid-angle and modular γ detectors can be built. The Crystal Barrel collaboration at LEAR is investigating low energy annihilation into final states involving several neutral particles (π^0, η, η',

ω). The detection of the 2γ decay modes (or 3γ for the ω) not only provides strong constraints in the event reconstruction (through kinematical fitting), but also avoids the serious combinatorial background of final-states charged pions for the η and ω decay mode $\pi^+\pi^-\pi^0$. Furthermore, the amplitude analysis for final states involving neutral pion pairs is generally simpler than for those involving $\pi^+\pi^-$ pairs, since the strongly produced ρ^0 meson does not decay into $\pi^0\pi^0$, and since C-parity conservation reduces the number of contributing $\bar{p}p$ initial states.

The main motivation for light quark spectroscopy is to search for mesons that are not made of $\bar{q}q$ pairs (glueballs, hybrid mesons, multiquark states, two-meson molecules, or $\bar{N}N$ states). (For recent reviews, see 16, 17.) Since $\bar{p}p$ annihilation is a good source of gluons, one expects to produce some of these states in addition to the standard quark model $\bar{q}q$ states. Therefore both initial and final states must be carefully selected to enhance the signals. At rest, only a few initial states can contribute, depending on the final state (0^{-+}, 1^{--} for initial S states and 0^{++}, 1^{++}, 2^{++}, and 1^{+-} for initial P states). However, phase space limits the accessible mass range to a maximum of $\sim$1650 MeV. Higher masses can be reached by $\bar{p}p$ annihilation in flight, but then many partial waves contribute in the initial state.

Although we do not have any straightforward recipe to identify exotic mesons, guidelines are well established. For example, for gluonic hadrons the relevant decay modes are those involving strange quarks ($\eta\eta$, $\eta\eta'$, and $\bar{K}K$) since gluons are flavor blind. Also, decay channels with quantum numbers 0^{--}, 0^{+-}, 1^{-+}, 2^{+-}, etc, which do not couple to $\bar{q}q$, are useful to identify exotic particles unambiguously, for instance the decay modes $\omega\pi$ and $\omega\eta$, which can couple to 0^{--}, or $\eta\pi$ and $\eta\eta'$, which can couple to 1^{-+}. A 1^{-+} state at 1405 MeV, decaying to $\eta\pi$, was recently reported by the GAMS collaboration at CERN (177).

Finally, all the $\bar{q}q$ states need to be identified. In the mass range accessible to annihilation at rest, essentially only S- and P-wave $\bar{q}q$ mesons need to be considered. These are the nonets 0^{-+}, 1^{--}, 1^{+-}, 0^{++}, 1^{++}, 2^{++} and their radial excitations. In quark model spectroscopy, a principal problem is the mass assignment for the radially excited S-state $\bar{q}q$ mesons. We know that the 2S $\bar{q}q$ state can be lower in mass than the lightest $\bar{q}q$ P state if the (u,d,s) quarks experience an attractive Yukawa-like force (178). An example of an unusual mass ordering is the $J^P = 1/2^+$ Roper resonance N*(1440), which is lighter than the lightest negative-parity state N(1520) with $J^P = 3/2^-$. This unusual mass ordering cannot be explained with power law quark potentials (179). Baryons are not mesons; nevertheless one might have several radially excited $\bar{q}q$ mesons in the 1–2 GeV mass range.

The scalar meson nonet is not well established because the $a_0(980)$ and $f_0(975)$ are believed to be $\bar{K}K$ molecules (180). Instead, the scalar isovector $\bar{q}q$ meson of the 0^{++} nonet could be the $a_0(1320)$ decaying to $\eta\pi$, reported by the GAMS collaboration (181), while one of the isoscalar mesons could be the (nearly pure) $\bar{s}s$ meson $f_0(1525) \rightarrow \bar{K}K$ reported by LASS (182). In addition, there is the excess candidate $f_0(1590) \rightarrow \eta\eta$, $\eta\eta'$, $4\pi^0$ (183; for review, see 17). However, these states need confirmation. In the axial vector meson nonet, the missing 1^{+-} isoscalar is reported by LASS at 1380 MeV, decaying to $K\bar{K}^*$ (184). The 1^{++} states are discussed by Burnett & Sharpe (17). There are two candidates for the $\bar{s}s$ 1^{++} states, $f_1(1420)$ and $f_1(1510)$. The latter fits better in the nonet, assuming ideal mixing. The former might be an exotic state (see 17). The excited η and f_2 mesons are discussed below.

Above $\sim$1650 MeV the experimental situation is very confused. All nonets are incomplete (with the possible exception of 3^{--}) although many candidates exist.

4.2 *Recent Results in $\bar{p}p$ Annihilation*

4.2.1 THE E MESON The E(1420) was first discovered in $\bar{p}p$ annihilation at rest in liquid into $(K^{\pm}K_s\pi^+)\pi^+\pi^-$. Its quantum numbers had been determined to be 0^{-+} (173). However, this assignment has been the subject of a long controversy. Several experiments (inelastic πp, pp central collisions, and $\gamma\gamma$ collision) report either a 0^{-+} (185, 186) or a 1^{++} state [$f_1(1420)$] (187–189) at the same mass. [Following an early observation of a 1^{++} state at 1420 MeV (187), the E meson was renamed $f_1(1420)$ by the Particle Data Group. As we argue below, the renaming is not justified.] Furthermore, a glueball candidate around 1440 MeV, $\eta(1440)$ (formerly ι), is observed in radiative J/ψ decay. The question naturally arises as to whether the states observed in $\bar{p}p$ annihilation and in J/ψ decay are identical. According to a recent analysis by the Mark III collaboration, the $\eta(1440)$ is made of three states, $f_1(1443)$, $\eta(1416)$, and $\eta(1490)$ (190).

The Asterix collaboration confirmed the original 0^{-+} assignment for the E meson, but with a hydrogen gas target (191). Figure 8*a* shows the $K^{\pm}K^0\pi^{\mp}$ invariant mass distribution. The charged $K^{\pm}$ was detected by ionization sampling while the neutral $K^0(\overline{K^0})$ here was a K_L escaping detection or a $K_S \rightarrow \pi^0\pi^0$. Since there are two possible combinations for the $\pi^{\mp}$, the wrong-charge invariant mass distribution $K^{\mp}K^0\pi^{\mp}$ (one entry per event) was subtracted from the $K^{\pm}K^0\pi^{\mp}$ (two entries per event). The peak with mass 1413 ± 8 MeV and width 62 ± 16 MeV is fully consistent with the original E(1420) (173). In addition, a 3σ peak is seen, consistent with the well-known $f_1(1285)$, which was not observed earlier in liquid (173). A Dalitz plot analysis of the E meson was attempted but one could

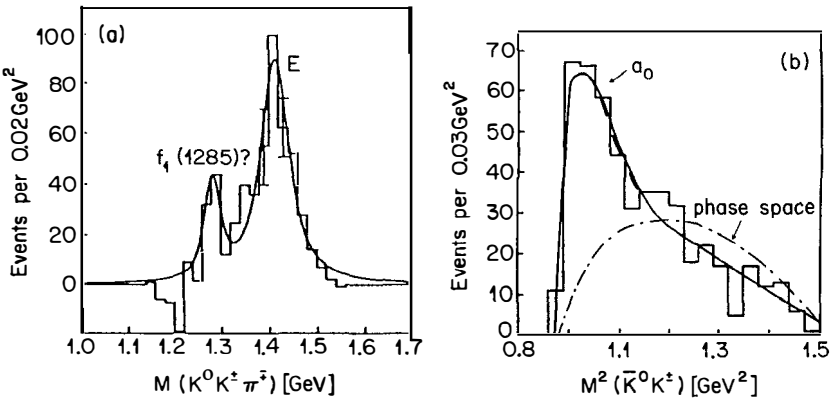

Figure 8 (*a*) Distribution of $K^0K^-\pi^+$ invariant mass (+c.c.) in $\bar{p}p \rightarrow K^0K^-\pi^+\pi^+\pi^-$ (+c.c.). (*b*) K^0K^- invariant mass (+c.c.) in the E meson region (191, 192).

not distinguish between 0^{-+} and 1^{++} (191). The dominant decay mode for the E meson is $a_0(980)\pi$ [$a_0(980) \rightarrow \bar{K}K$], at variance with the $K\bar{K}^*$ decay mode of the $f_1(1420)$ (Figure 8*b*) and in agreement with the decay mode of $\eta(1440)$ found in radiative J/ψ decay.

The 0^{-+} assignment can nevertheless be established from the E meson production rate, as a 1^{++} state cannot be produced with a pair of pions from $\bar{p}p$ S states: because of the limited phase space, a 0^{++} di-pion recoils against the E meson with zero relative angular momentum. Hence the 0^{-+} E meson is produced from the $^1S_0$ $\bar{p}p$ state. A 1^{++} meson [like $f_1(1285)$] would be produced mainly from the $^3P_1$ state and hence should not be seen in liquid, as confirmed by the earlier data (173). If this phase-space argument holds, then the 0^{-+} E meson should be produced from P states while $f_1(1285)$ should be prominent. The branching ratio for $\bar{p}p \rightarrow (E \rightarrow K^\mp K^0\pi^\pm)\pi^+\pi^-$ is $(7.1 \pm 0.4) \times 10^{-4}$ in liquid (173). In the gas target (Figure 8), the fraction of P wave is 61% and the branching ratio is $(3.0 \pm 0.9) \times 10^{-4}$ (191). With these two measurements one extrapolates to 100% P wave and finds that the branching ratio is consistent with zero, i.e. the E meson is 0^{-+}.

A similar suppression also operates for the pseudoscalars in the channels $\bar{p}p \rightarrow \eta\pi^+\pi^-$ and $\eta'\pi^+\pi^-$ (see Section 3.1.3 and Table 2). The phase-space suppression is, of course, less dramatic than for $E\pi\pi$ since η and η' are lighter than the E meson.

4.2.2 THE $f_2(1565)$ IN ITS $\pi^+\pi^-$ DECAY MODE As discussed in Section 3.1.2, the Asterix collaboration has presented new data (119) for $\bar{p}p$ annihilation into $\pi^+\pi^-\pi^0$ in gaseous hydrogen (53% P wave) and in off-line coincidence

with L x rays (92% P wave) (see Figure 6). Apart from ρ^0 and $f_2(1270)$, a new resonance $f_2(1565)$ (called AX by the collaboration) is observed to decay into $\pi^+\pi^-$ from P states.

Since $f_2(1565) \to \pi^+\pi^-$ and no charged partner is observed in $\pi^\pm\pi^0$, the quantum numbers are $J^{PC}(I^G) = 0^{++}$ or 2^{++} (0^+). Higher even spins are not expected at this low mass. Without $f_2(1565)$ the fit is poor. A better fit is obtained with a 2^{++} (or a 0^{++}) state with mass 1565 ± 20 MeV and width of 170 ± 40 MeV. The analysis is complicated by the occurrence of $\rho^+\rho^-$ interference under the $f_2(1565)$, which could shift the mass and change the width of this meson. Since 2^{++} is preferred by the fit, but 0^{++} is not excluded, a phase-shift analysis was performed. The relativistic Breit-Wigner amplitude for $f_2(1565)$ was parametrized by the amplitude ae^{ib}, which was allowed to interfere with the other amplitudes describing the Dalitz plot. The 2^{++} phase advances through 90° at the correct $\pi^+\pi^-$ mass and it is concluded that a new isoscalar 2^{++} state has been observed (119). The branching ratio for $\bar{p}p \to f_2(1565)\pi^0$ with $f_2(1565) \to \pi^+\pi^-$ is $(3.7 \pm 0.6) \times 10^{-3}$, and $f_2(1565)$ is produced mainly from the isovector 1^{++} and 2^{++} $\bar{p}p$ states while $f_2(1270)$ is produced dominantly from 1^{++} (see Table 3).

4.2.3 THE $f_2(1565)$ IN ITS $\rho^0\rho^0$ DECAY MODE A state (called ζ) with mass 1477 and width 116 MeV was reported from bubble chamber exposures in the reaction $\bar{p}n \to (\zeta \to 2\pi^+2\pi^-)\pi^-$, where the momentum of the spectator proton was less than 200 MeV/c (193). The ζ peak is best seen by subtracting the wrong-charge invariant mass $(3\pi^-\pi^+)\pi^+$ distribution (two combinations per event) from the $(2\pi^+2\pi^-)\pi^-$ distribution (three combinations per event) as shown in Figure 9. An amplitude analysis of the five-pion system led to the spin-parity 2^{++} and $\zeta \to \rho^0\rho^0$. The branching ratio for production and decay into $\rho^0\rho^0$ is $3.7 \pm 0.3\%$. The isospin is presumably zero since $I = 1$ does not couple to $\rho^0\rho^0$. For $I = 2$, the decay rate into $\rho^+\rho^-$ can be related to $\rho^0\rho^0$ by Clebsch-Gordan coefficients. With $I = 2$ the rate for production and decay into $\rho^0\rho^0 + \rho^+\rho^-$ would be 50% of all $\bar{p}n$ annihilations, an unreasonably high branching ratio.

The Asterix collaboration has confirmed the existence of an enhancement compatible with $\rho^0\rho^0$ decay at the mass 1504 MeV with a width of 206 MeV for the same reaction in gaseous deuterium with five times more events (121, 194). No spin-parity analysis has been performed. These data are also shown in Figure 9. However, the mass and width of the enhancement depend on the spectator momentum, as demonstrated by the Asterix data (Figures 9*b*,*c*). Higher spectator momenta are associated with a lower resonance mass (Figure 9*c*). The contribution from pion rescattering (inset of Figure 9*b*) has been calculated (195). The scattering

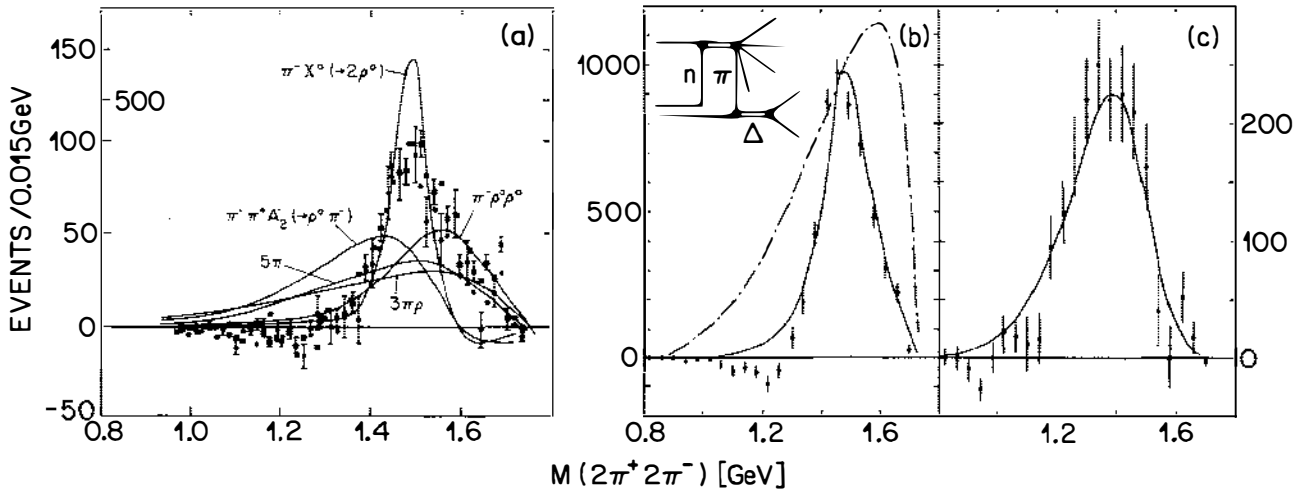

Figure 9 (*a*) Distribution of invariant $2\pi^+2\pi^-$ mass in $\bar{p}n \rightarrow 3\pi^-2\pi^+$ after subtraction of the wrong combinations (see text). The circles (error bars omitted for clarity) are from Bridges et al (193) and the squares (with error bars) from the Asterix collaboration (192, 194). The data from (*a*) are shown with (*b*) low (<200 MeV/c) and (*c*) high (>200 MeV/c) proton spectator momentum. The solid lines in (*b*) and (*c*) show the rescattering prediction, and the dashed-dotted line in (*b*) shows the prediction without ζ resonance (195).

of one of the ρ decay pions leads to a lower $\rho\rho$ invariant mass and boosts the "spectator" proton to higher momenta. The prediction is in excellent agreement with data.

Since $f_2(1565)$ and ζ have the same quantum numbers, both are produced from $I = 1$ $\bar{p}N$ states, and their masses and widths are comparable, one concludes that the states are probably identical. As discussed in the next section, the mass of $f_2(1565)$ may actually be close to 1515 MeV as observed in its $\pi^0\pi^0$ decay mode. Notice that $f_2(1565)$ is produced from P states only, which implies that P wave in $\bar{p}n$ annihilation in deuterium should be strong, even for low spectator momenta, or alternatively, much stronger in the $I = 1$ than in the $I = 0$ states. This is supported by the large $f_2(1270)$ production rate in $\bar{p}n \to \pi^+\pi^-\pi^-$ (130) and in the $(I = 1)$ $3\pi^0$ final state (next section). The rate R for $\pi^-\pi^0$ on the neutron should be twice the rate for $\pi^+\pi^-$ on the proton if S wave dominates annihilation into $\pi\pi$ [after correcting for the ratio of $\bar{p}p$ to $\bar{p}n$ annihilation in deuterium: 1.33 ± 0.07 (196)]. A recent measurement in a liquid deuterium target at LEAR indeed finds $R = 2.07 \pm 0.05$ (197), which is at variance with an earlier measurement that led to $R = 0.68 \pm 0.07$ (198), and which therefore disputed the S-wave dominance. However, these measurements (197, 198) apply to the fraction of P and S waves for annihilation into 2π, not necessarily into 3π or 5π.

The need for $\rho\rho$ resonances in the five-pion channels is not new. A 2^{++} (0^+) $\rho^0\rho^0$ resonance was introduced earlier to obtain satisfactory fits to $2\pi^+2\pi^-\pi^0$ in $\bar{p}p$ annihilation at rest (199).

4.2.4 THE $f_2(1565)$ IN ITS $\pi^0\pi^0$ DECAY MODE The Crystal Barrel collaboration at LEAR has presented new data on the annihilation channel $\bar{p}p \to \pi^0\pi^0\pi^0$ at rest in liquid hydrogen (200). The Crystal Barrel detects charged particles over a solid angle of $95\% \times 4\pi$ and photons with 100% efficiency over $97\% \times 4\pi$. The 200-MeV/c antiprotons enter a solenoid magnet and annihilate in a liquid hydrogen target. Two cylindrical proportional wire chambers provide the trigger for the final-state charged multiplicity (here zero prong). Photons are detected in a barrel-shaped assembly of 1380 CsI(Tl) crystals with photodiode readout. Details on the apparatus can be found in the paper by Aker et al (201).

The $3\pi^0$ Dalitz plot and its projection are shown in Figure 10. One observes three bands corresponding to $f_2(1270) \to \pi^0\pi^0$ interfering at the edge of the Dalitz plot. The additional three bands correspond to a state around 1515 MeV decaying into $\pi^0\pi^0$. A Dalitz plot analysis has been performed including the contributing 0^{-+} (S-wave) and the 1^{++} and 2^{++} (P-wave) $\bar{p}p$ initial states. The energy-dependent amplitudes of Au et al (202) were introduced into the fit to describe the 0^{++} $\pi^0\pi^0$ partial wave.

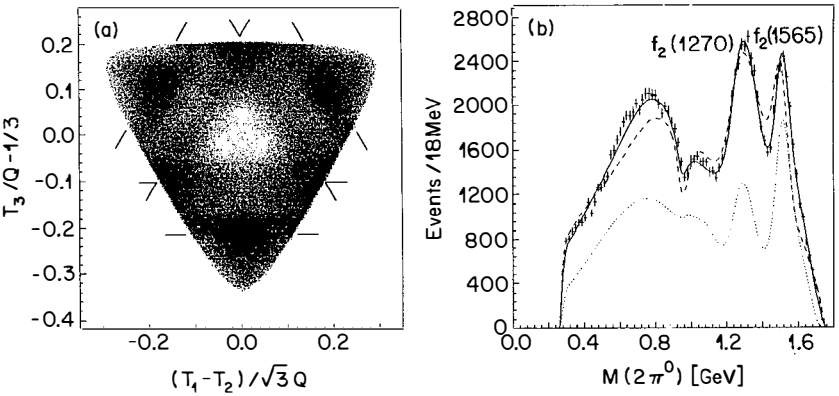

Figure 10 (*a*) Dalitz plot for the reaction $\bar{p}p \to 3\pi^0$. The marks indicate the $f_2(1565)$ bands (corners of the plot) and the $f_2(1270)$ bands (interfering at the edge of the plot). (*b*) Distribution of $\pi^0\pi^0$ invariant mass. The dotted line shows the total $\bar{p}p$ P-wave contribution, the dashed line shows the fit for a 2^{++} state at 1515 MeV, and the full curve includes the tail of $f_2(1810)$ (200).

A 0^{++} resonance at 1515 MeV does not describe the data (200). The dashed line in Figure 10*b* shows the fit for a 2^{++} resonance; the full curve shows the same fit but includes the broad $f_2(1810)$ observed earlier in the partial wave analysis of K^-K^+ and $\pi^-\pi^+$ (203). The various contributions are given in Table 4.

One concludes that a tensor meson with mass 1515 ± 10 MeV and width 120 ± 10 MeV is observed. This state is probably identical to $f_2(1565)$, although the mass and width are slightly lower. However, in contrast to $\pi^+\pi^-\pi^0$, the difficulty of the interfering $\rho^+\rho^-$ bands below the $f_2(1565)$ is avoided. Therefore, the mass and width obtained in this experiment are more reliable. The state at 1515 MeV is produced from $^1S_0$, $^3P_1$, and $^3P_2$ with comparable rates (Table 4). The sizeable contribution from $^1S_0$ is not in contradiction with Asterix data since the branching ratio for $\bar{p}p \to 3\pi^0$

Table 4 Contribution (in %) to $\bar{p}p$ annihilation into $3\pi^0$ in liquid hydrogen (200)[a]

	$^1S_0$	$^3P_1$	$^3P_2$
$\pi^0\pi^0$-S wave	28.3 ± 2.5		
$f_2(1270)\pi^0$	2.9 ± 1.1	19.3 ± 1.1	
$f_2(1565)\pi^0$	9.5 ± 0.7	8.0 ± 0.5	8.8 ± 1.1
$f_2(1810)\pi^0$			23.2 ± 2.5

[a] The branching ratio for $\bar{p}p \to 3\pi^0$ is $0.76 \pm 0.23\%$ (204).

in liquid hydrogen is only $0.76 \pm 0.23\%$ (204), compared to $6.6 \pm 0.8\%$ for $\pi^+\pi^-\pi^0$ in liquid (119). Hence the S-wave contribution to $f_2(1565)$ computed from the $3\pi^0$ data is expected to be tiny in the charged channel and further hidden under the $\rho^+\rho^-$ interference. In addition, both $f_2(1270)$ and $f_2(1565)$ are strongly produced from P states, although liquid hydrogen is used in the Crystal Barrel. This is also not a contradiction since the $3\pi^0$ final state is exclusively $I = 1$ while $\pi^+\pi^-\pi^0$ is dominantly $I = 0$ (119). One therefore expects that the $f_2(1565)$ signal will be hidden below the strong $I = 0$ background in liquid hydrogen.

Enhancements around 1500–1600 MeV in $\pi^+\pi^-$ and $\pi^0\pi^0$ have been reported earlier in $\bar{p}n \to \pi^+\pi^-\pi^-$ (129) and $\bar{p}p \to 3\pi^0$ (129, 204) albeit with limited statistics. The meson $f_2(1565)$ is not $f_2'(1525)$ since the production branching ratio for $\bar{p}p \to f_2(1565)\pi^0$ at rest would be $\sim 50\%$, $f_2'(1525)$ decaying mainly to $\bar{K}K$. In fact, no signal is observed in $\bar{K}K$ (129). The 2^{++} $\bar{q}q$ ground-state mesons are known and the first radial excitation is predicted around 1820 MeV (205), although the mass of a radial excitation is very model dependent and difficult to calculate (Section 4.1). The state $f_2(1515)$ is a candidate for the first radial excitation. This state could be, if not a radial excitation, a glueball, a hybrid, a $\bar{q}^2q^2$ state (206), or an $\bar{N}N$ molecule (141). Furthermore, $I = 1$ or $I = 2$ states are not observed by Asterix in the $\pi^\pm\pi^0$ invariant mass (Figure 6).

A natural parity band of $I = 0$ $\bar{N}N$ molecular states is predicted by potential models (161). If $f_2(1565)$ is the 2^{++} member of this band, then 1^{--} and 0^{++} states are expected around 1250 and 1100 MeV respectively (141). Candidates for these states have been reported. A scalar state decaying into two pions is suggested at this mass in the final states $\omega\pi^+\pi^-$ (103), $\rho^0\pi^+\pi^-$ (207), and in $\bar{p}n - \rho^-\pi^+\pi^-$ (208). A vector meson has also been reported at 1250 MeV in $\bar{p}p \to (e^+e^-)X$ (209), although with very limited statistics. For further theoretical considerations, see the reviews (16, 17).

5. ANTIPROTON-NUCLEUS INTERACTIONS

The antiproton interacts only with the nuclear surface at a maximum of 10% of the central nuclear density. The interior of the nucleus is black to antiprotons, which means that the short-range (heavy-meson) exchanges in the $\bar{N}N$ potential will be partially absorbed because of the nuclear density, and the longer-range (OPE) will be the dominant exchange. Therefore, in inelastic $(\bar{p}, \bar{n})$ nuclear reactions, the pionlike states (0^-, 1^+, 2^-, etc) should be preferentially excited, as opposed to the many more states in (n, p) reactions. This is one of the useful aspects of antiproton-nucleus reaction studies. So far this type of experiment has not been performed.

The experimental data in antiproton-nucleus interactions have been reviewed by Guaraldo (210).

The antiproton-nucleus interaction is successfully described by the intranuclear cascade model (INC); see the review by Cugnon & Vandermeulen (211). The momentum distribution of pions following $\bar{p}$ annihilation on a nucleus shows two apparent temperature scales, $T \sim 100$ MeV and $T \sim 50$ MeV (211, 212). The first temperature is associated with $\bar{N}N$ annihilation (Section 3.3), the other is associated with pion rescattering from nucleons, which also leads to a proton momentum spectrum with a high energy tail. These distributions are reproduced in the cascade calculations (211). Furthermore, these calculations find that, after a few energetic protons remove some 200 MeV, the nucleus loses excitation energy by evaporating a few nucleons or fragmenting into many pieces. For a more detailed discussion, see the review by Cugnon & Vandermeulen (211).

It has been speculated that the production of strangeness (for example, the production of kaons and hyperons) could be enhanced in $\bar{p}$-nucleus annihilation either by the formation of quark-gluon plasma (213) or by annihilation on a cluster of several nucleons. The fraction of strangeness production measured in the ITEP xenon bubble chamber is $6.2 \pm 0.9\%$ for antiprotons at rest and $6.2 \pm 0.8\%$ in the 0.4–0.9 GeV/c range (214). The value obtained in an INC calculation is 6.25% at 0.65 GeV/c (215). Rescattering of annihilation mesons, mainly strangeness exchange ($\bar{K}N \rightarrow \Lambda\pi$), accounts for the observed Λ production on several nuclei (215, 216). Hence no unusual yield is observed in strangeness production for low energy $\bar{p}$-nucleus annihilation.

The so-called Pontecorvo reaction $\bar{p}d \rightarrow \pi^- p$ occurs with a rate $\sim 2 \times 10^{-5}$ (196, 217, 218). It is not clear which process (rescattering or multiquark clusters) dominates this interaction since the interpretation is model dependent. There are two calculations of the rescattering contributions for this reaction, one finding a rate of the right order of magnitude but with large theoretical uncertainties (219), the other finding too small a rate (220). The relative rates for other Pontecorvo reactions (such as $\bar{p}d \rightarrow \pi^- p$, $\Sigma^- K^+$, $K^0\Lambda$) are less model dependent, but unfortunately no data exist except for $\pi^- p$.

6. OUTLOOK

A wealth of interesting new data has emerged from the LEAR facility. Some of the low energy scattering data can be readily understood by effective meson-baryon models. Other measurements might require a treatment of QCD in the nonperturbative regime. The scattering and annihil-

ation data are still quite fragmentary. However, the first round of LEAR experiments provides guidelines as to which phenomena should be studied next. For example, the peculiar oscillatory behavior of the ρ parameter below 200 MeV/c should be studied at LEAR with a gaseous hydrogen target.

We have shown that polarization measurements are sensitive to the behavior of the interaction at short distances. Apart from the analyzing power data at a few energies, we do not have precise measurements of other spin observables. These experiments require intense polarized antiproton beams and good analyzers of antiproton polarization. However, a few observables such as spin correlations can possibly be measured with an internal polarized antiproton beam and a polarized hydrogen gas jet (221). Polarization effects should be investigated in the charge exchange reaction and in (the pure $I = 1$) elastic $\bar{n}p$ scattering for which only measurements of the total cross section and of integrated annihilation cross sections are available (222, 223).

The charge exchange reaction is unique since it is the only NN or $\bar{N}N$ reaction where we can measure the *difference* of the two large isospin amplitudes in order to probe the isovector part of the meson exchange forces. This reaction is a critical test of the models used to explain the data. For example, for the charge exchange reaction, a very large transfer of longitudinal polarization from the proton to the antineutron is predicted in the forward direction (224), a feature that could be used to generate polarized antineutron beams. Present experimental results at the lower energies show that our model understanding is reasonable, and further specific polarization measurements could be very beneficial to our understanding of these reactions and the intermediate-range $\bar{N}N$ (and possibly NN) forces.

For $\bar{p}p$ and $\bar{n}p$ annihilation, the Crystal Barrel and Obelix experiments will provide the large data samples of neutral and kaonic final states required to study both the annihilation dynamics and the production of new and possibly exotic mesons. The study of specific two-body annihilation reactions in flight has been limited so far. Two-body differential cross sections as a function of momentum are only available for $\pi^-\pi^+$, K^-K^+ (142, 144–146, 150), and $\pi^0\pi^0$, $\pi^0\eta$ (225) above 1 GeV/c. A partial wave amplitude analysis of these reactions has been performed and shows resonance behavior in nearly all partial waves (226). These resonances cannot be observed in the total annihilation cross section because of the dominating nonresonant background. Both reactions $\bar{p}p \to K^-K^+$ and $\pi^-\pi^+$ possess the dramatic property of a maximum left-right asymmetry in a wide angular range. Other two-body final states ($\pi^0\omega$, $\omega\omega$, $\eta\omega$, K_SK_S, K_SK_L, etc), possibly with a polarized target, should be systematically

studied to clarify the dynamics involved in these reactions. In addition, the glueball-sensitive channels like $\phi\phi$ (row being studied by the Jetset collaboration) are accessible at LEAR, but only in a very narrow energy window limited by threshold (2.04 GeV) and the maximum available center-of-mass energy of 2.4 GeV.

At LEAR, the accessible mass range for the production of meson resonances, associated with the emission of one or two pions, is limited by phase space. Hence glueballs or hybrids might not be observed in production at LEAR, if their masses lie above 2 GeV or if they are broad and lie in the mass range 1.7 to 2 GeV. The formation and production of exotic light quark mesons might be investigated at the SuperLEAR facility that is currently being evaluated, or with antiprotons at the KAON factory.

Charmonium states ($\bar{c}c$) or charmed hybrids ($\bar{c}cg$) (227) might be studied in formation at the SuperLEAR facility. In parallel, antiprotons interacting with nuclei could be used to investigate the formation and interaction of J/ψ in nuclear matter (important in relativistic heavy-ion searches for the quark-gluon plasma), in charmonium-nucleus bound states, and in charmed hypernuclei, as well as to test the hypothesis of color transparency (228, 229).

ACKNOWLEDGMENT

We thank Prof. J. Vandermeulen for useful discussions related to the antiproton-nucleus interaction. This work was supported in part by a grant from the National Science Foundation (FM).

Literature Cited

1. Walcher, Th., *Annu. Rev. Nucl. Part. Sci.* 38: 67–95 (1988)
2. Kerbikov, B. O., Kondratyuk, L. A., Sapozhnikov, M. G., *Sov. Phys. Usp.* 32: 739 (1989)
3. Sedlak, J., Simak, V., *Sov. J. Part. Nucl.* 19: 191 (1988)
4. DeGrand, T., et al., *Phys. Rev.* D12: 2060 (1975)
5. Close, F. E., *An Introduction to Quarks and Partons.* New York: Academic (1979)
6. Isgur, N., Karl, G., *Phys. Rev.* D18: 4187 (1978); D19: 2653 (1979)
7. Thomas, A. W., *Adv. Nucl. Phys.* 13: 1 (1983)
8. Myhrer, F., In *Quarks and Nuclei, Int. Rev. Nucl. Phys.*, ed. W. Weise. Singapore: World Scientific (1984), 1: 325–407
9. Bryan, R. A., Phillips, R. J. N., *Nucl. Phys.* B5: 201 (1968)
10. Dover, C. B., Richard, J. M., *Phys. Rev.* C21: 1466 (1980)
11. Dalkarov, O. D., Myhrer, F., *Nuovo Cimento* 40A: 152 (1977)
12. Myhrer, F., *Nucl. Phys.* A508: 513c (1990)
13. Serber, R., *Phys. Rev. Lett.* 10: 357 (1963)
14. Brückner, W., et al., *Phys. Lett.* B166: 113 (1986); CERN-PPE preprint 91-41 (1991)
15. Anderson, B., et al., *Phys. Rep.* 97: 33 (1983)
16. Close, F. E., *Rep. Prog. Phys.* 51: 833 (1988)
17. Burnett, T. H., Sharpe, S. R., *Annu. Rev. Nucl. Part. Sci.* 40: 327–55 (1990)
18. Amsler, C., *Adv. Nucl. Phys.* 18: 183 (1987)
19. Myhrer, F., Wroldsen, J., *Rev. Mod. Phys.* 60: 629 (1988)

20. Vinh Mau, R., et al., *Phys. Lett.* B44: 1 (1973)
21. Ericson, T. E. O., Rosa-Clot, M., *Annu. Rev. Nucl. Part. Sci.* 35: 271–94 (1985)
22. Lacombe, M., et al., *Phys. Rev.* D12: 1495 (1975)
23. Brown, G. E., Jackson, A. D., *Nucleon-Nucleon Interaction.* Amsterdam: North-Holland (1976)
24. Machleidt, R., Holinde, K., Elster, Ch., *Phys. Rep.* 149: 1 (1987)
25. Hamilton, J., Oades, G. C., *Nucl. Phys.* A424: 447 (1984)
26. Nagels, M. M., Rijken, T. A., de Swart, J. J., *Phys. Rev.* D12: 744 (1975); D15: 2547 (1977); D17: 768 (1978)
27. Oka, M., Yazaki, K., See Ref. 8, 1: 489–568
28. Phillips, R. J. N., *Rev. Mod. Phys.* 39: 681 (1967)
29. Kimura, M., Saito, S., *Nucl. Phys.* B178: 477 (1981); Kim, J. H., Toki, H., *Prog. Theor. Phys.* 78: 616 (1987); Gregory, P., et al., *Nucl. Phys.* B102: 189 (1976)
30. Pais, A., *Ann. Phys. NY* 9: 548 (1960)
31. Fett, E., et al., *Nucl. Phys.* B130: 1 (1977)
32. Vandermeulen, J., *Z. Phys.* C37: 563 (1988)
33. Martin, A., *Phys. Rev.* 124: 614 (1961)
34. Côté, J., et al., *Phys. Rev. Lett.* 48: 1319 (1982)
35. Hippchen, T., Holinde, K., Plessas, W., *Phys. Rev.* C39: 761 (1989)
36. Tegen, R., Mizutani, T., Myhrer, F., *Phys. Rev.* D32: 1672 (1985)
37. Moussallam, B., *Nucl. Phys.* A407: 413 (1983); A429: 429 (1984)
38. Hippchen, T., et al., *Nucl. Phys. B. Proc. Suppl.* 8: 116 (1989); Hippchen, T., et al., Jülich preprint KFA-IKP(TH)-1991-3 (1991); *Phys. Rev. C.* In press (1991)
39. Liu, G. Q., Tabakin, F., *Phys. Rev.* C41: 665 (1990)
40. Holinde, K., et al., In *First Biennial Conf. on Low Energy Antiproton Physics*, ed. P. Carlson, et al. Singapore: World Scientific (1991), p. 92
41. Dalkarov, O. D., Mandelzweig, V. B., Shapiro, I. S., *JETP Lett.* 10: 257 (1969); *Nucl. Phys.* B21: 88 (1970)
42. Montanet, L., Rossi, G. C., Veneziano, G., *Phys. Rep.* 63: 149 (1980)
43. Myhrer, F., *AIP Conf. Proc.* 41: 357 (1978)
44. Myhrer, F., Gersten, A., *Nuovo Cimento* 37A: 21 (1977)
45. Myhrer, F., Thomas, A. W., *Phys. Lett.* B64: 59 (1976)
46. Shibata, T.-A., *Phys. Lett.* B189: 232 (1987)
47. Haidenbauer, J., et al., *Z. Phys.* A334: 467 (1989); *Nucl. Phys.* A508: 329c (1990)
48. Shapiro, I. S., *Phys. Rep.* 35: 129 (1978)
49. Shapiro, I. S., *Nucl. Phys. B. Proc. Suppl.* 8: 100 (1989)
50. Clough, A. S., et al., *Phys. Lett.* B146: 299 (1984)
51. Bugg, D. V., et al., *Phys. Lett.* B194: 563 (1987)
52. Brückner, W., et al., *Z. Phys.* A335: 217 (1990)
53. Brückner, W., et al., *Phys. Lett.* B169: 302 (1985)
54. Agnello, M., et al., *Phys. Lett.* B256: 349 (1991)
55. Kroll, P., Schweiger, W., *Nucl. Phys.* A503: 865 (1989)
56. Brückner, W., et al., *Phys. Lett.* B197: 463 (1987)
57. Kunne, R., et al., *Nucl. Phys.* B323: 1 (1989)
58. Bertini, R., et al. *Phys. Lett.* B228: 531 (1989)
59. Tegen, R., Myhrer, F., Mizutani, T., *Phys. Lett.* B182: 6 (1986)
60. Kohno, M., Weise, W., *Nucl. Phys.* A454: 429 (1986); *Phys. Lett.* B152: 303 (1985)
61. Linsen, L., et al., *Nucl. Phys.* A469: 726 (1987)
62. Brückner, W., et al., *Phys. Lett.* B158: 180 (1985)
63. Schiavon, P., et al., *Nucl. Phys.* A505: 595 (1989)
64. Batty, C. J., *Rep. Prog. Phys.* 52: 1165 (1989)
65. Kroll, P., Schweiger, W., *Nucl. Phys. B. Proc. Suppl.* 8: 121 (1989)
66. Fasano, C. G., Locher, M. P., *Z. Phys.* A336: 469 (1990)
67. Mahalanabis, J., Pirner, H. J., Shibata, T.-A., *Nucl. Phys.* A 485: 546 (1988)
68. Kunne, R., et al., *Phys. Lett.* B206: 557 (1988)
69. Timmers, P. H., van der Sanden, W. A., de Swart, J. J., *Phys. Rev.* D29: 1928 (1984)
70. Birsa, R., et al., *Phys. Lett.* B246: 267 (1990)
71. Perrot-Kunne, F., See Ref. 40, p. 251
72. Bradamante, F., See Ref. 40, p. 219
73. Martin, A., et al., *Nucl. Phys.* A487: 563 (1988)
74. Kunne, R. A., et al., See Ref. 40, p. 241
75. Nakamura, K., et al., *Phys. Rev. Lett.* 53: 885 (1985)
76. Hamilton, R. P., et al., *Phys. Rev. Lett.* 44: 1179 (1980)
77. Barnes, P. D., et al., *Phys. Lett.* B189: 249 (1987)

78. Barnes, P. D., et al., *Phys. Lett.* B229: 432 (1989)
79. Barnes, P. D., et al., *Nucl. Phys.* A526: 575 (1991)
80. Barnes, P. D., et al., *Phys. Lett.* B246: 273 (1990)
81. Kohno, M., Weise, W., *Nucl. Phys.* A479: 433c (1988); *Phys. Lett.* B179: 15 (1986); B206: 584 (1988)
82. Timmermans, R. G. E., Rijken, T. A., de Swart, J. J., *Nucl. Phys.* A479: 383c (1988)
83. Høgaasen, H., Høgaasen, J., *Nuovo Cimento* 40: 560 (1965)
84. Kaufmann, W. B., Pilkuhn, H., *Phys. Rev.* C17: 215 (1978)
85. Carbonell, J., Ihle, G., Richard, J. M., *Z. Phys.* A334: 329 (1989)
86. Reifenröther, G., Klempt, E., *Phys. Lett.* B245: 129 (1990)
87. Mandrup, L., et al., *Nucl. Phys.* A512: 591 (1990)
88. Jaenicke, S., Kerbikov, B., Pirner, H. J., *Z. Phys.* A339: 297 (1991)
88a. Schneider, M., et al., *Z. Phys.* A338: 217 (1991)
89. Batty, C. J., *Nucl. Phys.* A508: 89c (1990)
90. Green, A. M., Niskanen, J. A., *Prog. Part. Nucl. Phys.* 18: 93 (1987)
91. Armenteros, R., French, B., In *High Energy Physics*, ed. E. H. S. Burhop. London: Academic (1969), 4: 237
92. Day, T. B., Snow, G. A., Sucher, J., *Phys. Rev.* 3: 864 (1960)
93. Chiba, M., et al., *Phys. Rev.* D38: 2021 (1988); D39: 3227 (1989)
94. Adiels, L., et al., *Z. Phys.* C35: 15 (1987)
95. Adiels, L., et al., *Z. Phys.* C42: 49 (1989)
96. Bassompierre, G., et al., *Phys. Lett.* B64: 475 (1976)
97. Devons, S., et al., *Phys. Rev. Lett.* 27: 1614 (1971)
98. Bassompierre, G., et al., In *4th Eur. Antiproton Symp.*, ed. A. Fridman. Paris: CNRS (1978), I: 139
99. Chiba, M., et al., *Phys. Lett.* B202: 447 (1988)
100. Foster, M., et al., *Nucl. Phys.* B8: 174 (1968)
101. Espigat, P., et al., *Nucl. Phys.* B36: 93 (1972)
102. Baltay, C., et al., *Phys. Rev.* 145: 1103 (1966)
103. Bizzarri, R., et al., *Nucl. Phys.* B14: 169 (1969)
104. Smith, G. A., In *The Elementary Structure of Matter*, ed. J. M. Richard, et al. Berlin: Springer (1988), p. 197
105. Bloch, M., Fontaine, G., Lillestøl, E., *Nucl. Phys.* B23: 221 (1970)
106. Bizzarri, R., et al., *Nucl. Phys.* B27: 140 (1971)
107. Conforto, B., et al., *Nucl. Phys.* B3: 469 (1967)
108. Bettini, A., et al., *Nuovo Cimento* 63A: 1199 (1969)
109. Barash, N., et al., *Phys. Rev.* 145: 1095 (1966)
110. Doser, M., et al., *Nucl. Phys.* A486: 493 (1988)
111. Doser, M., et al., *Phys. Lett.* B215: 792 (1988)
112. Richard, J. M., Sainio, M. E., *Phys. Lett.* B110: 349 (1982)
113. Ahmad, S., et al., *Phys. Lett.* B157: 333 (1985)
114. Ziegler, M., et al., *Phys. Lett.* B206: 151 (1988)
115. Schaefer, U., et al., *Nucl. Phys.* A495: 451 (1989)
116. Ahmad, S., et al., *Nucl. Instrum. Methods* A286: 76 (1990)
117. Bettini, A., et al., *Nuovo Cimento* A62: 1038 (1969)
118. Foster, M., et al., *Nucl. Phys.* B6: 107 (1968)
119. May, B., et al., *Z. Phys.* C46: 191; C46: 203 (1990); *Phys. Lett.* B225: 450 (1989)
120. Weidenauer, P., et al., *Z. Phys.* C47: 353 (1990)
121. Weidenauer, P., et al., Personal communication (1991)
122. Ellis, J., Gabathuler, E., Karliner, M., *Phys. Lett.* B217: 173 (1989)
123. Dover, C. B., Fishbane, P. M., *Phys. Rev. Lett.* 62: 2917 (1989)
124. Close, F. E., Lipkin, H. J., *Phys. Rev. Lett.* 41: 1263 (1978); *Phys. Lett.* B196: 245 (1987)
125. Achasov, N. N., *JETP Lett.* 43: 526 (1986)
126. Bityukov, S. I., et al., *Phys. Lett.* B188: 383 (1987)
127. Reifenröther, G., et al., *Phys. Lett. B.* In press (1991)
128. Bizzarri, R., et al., *Nuomo Cimento* 20A: 393 (1974)
129. Gray, L., et al., *Phys. Rev.* D27: 307 (1983)
130. Bridges, D., et al., *Phys. Rev. Lett.* 56: 215 (1986)
131. Bettini, A., et al., *Nuovo Cimento* 67A: 642 (1967)
132. Bizzarri, R., et al., In *Physics at LEAR with Low-Energy Cooled Antiprotons*, ed. U. Gastaldi, R. Klapisch. New York: Plenum (1984), p. 193
133. Cooper, A. M., et al., *Nucl. Phys.* B146: 1 (1978)
134. Richter, B., et al., *Phys. Lett.* B126: 284 (1983)

135. Chiba, M., et al., *Phys. Lett.* B177: 217 (1986)
136. Adiels, L., et al., *Phys. Lett.* B182: 405 (1986)
137. Angelopoulos, A., et al., *Phys. Lett.* B178: 441 (1986)
138. Tauscher, L., In *Antiproton 86*, ed. S. Charalambous et al. Singapore: World Scientific (1987), p. 247
139. Angelopoulos, A., et al., *Phys. Lett.* B159: 210 (1985)
140. Ahmad, S., et al., *Phys. Lett.* B152: 135 (1985)
141. Dover, C. B., Gutsche, T., Faessler, A., *Phys. Rev.* C43: 379 (1991)
142. Tanimori, T., et al., *Phys. Rev.* D41: 744 (1990)
143. Tanimori, T., et al., *Phys. Rev. Lett.* 55: 1835 (1985)
144. Eisenhandler, E., et al., *Nucl. Phys.* B96: 109 (1975)
145. Birsa, R., et al., *Nucl. Phys. B. Proc. Suppl.* 8: 141 (1989)
146. Kochowski, C., et al., See Ref. 40, p. 173
147. Mull, V., et al., Jülich preprint KFA-IKP(TH)-1991-4 (1991); *Phys. Rev. C.* In press (1991)
148. Moussallam, B., In *Physics with Antiprotons at LEAR in the ACOL Era*, ed. U. Gastaldi et al. Singapore: Ed. Frontières (1985), p. 203
149. Mundigl, S., Vicente Vacas, M., Weise, W., *Nucl. Phys.* A523: 499 (1991)
150. Bardin, G., et al., *Phys. Lett.* B192: 471 (1987)
151. Maruyama, M., Ueda, T., *Prog. Theor. Phys.* 78: 841 (1987)
152. Dalpiaz, P., et al., See Ref. 40, p. 346
153. Dalkarov, O. D., Protasov, K. V., *Nucl. Phys.* A504: 845 (1989)
154. Chew, G. F., In *Proc. 14th Conf. on Physics*, Univ. Brussel. London: Wiley (1968), pp. 72–74
155. Dosch, H. G., Gromes, D., *Phys. Rev.* D33: 1378 (1986); *Z. Phys.* C34: 139 (1987)
156. Oades, G. C., et al., *Nucl. Phys.* A464: 538 (1987)
157. Martin, B. R., Morgan, D., See Ref. 98, 2: 101
158. Furui, S., et al., *Nucl. Phys.* A516: 643 (1990)
159. Povh, B., Walcher, Th., *Comments Nucl. Part. Phys.* 16: 85 (1986)
160. Mundigl, S., Vicente Vacas, M., Weise, W., *Z. Phys.* A338: 103 (1991)
161. Dover, C. B., Richard, J. M., *Ann. Phys. NY* 121: 47, 70 (1979)
162. Maruyama, M., et al., *Phys. Lett.* B215: 223 (1988)
163. Furui, S., *Nucl. Phys. B. Proc. Suppl.* 8: 231 (1989)
164. Klempt, E., *Phys. Lett.* B244: 122 (1990)
165. Mundigl, S., Vicente Vacas, M., Weise, W., *Nucl. Phys. B. Proc. Suppl.* 8. 228 (1989)
166. Genz, H., Martinis, M., Tatur, S., *Z. Phys.* A335: 87 (1990)
167. Hartmann, U., Klempt, E., Körner, J., *Z. Phys.* A331: 217 (1988)
168. Gutsche, T., Maruyama, M., Faessler, A., *Nucl. Phys.* A472: 643 (1987); A503: 737 (1989)
169. Kalashnikova, Yu. S., Yurov, V. P., *Phys. Lett.* B231: 341 (1989)
170. Henley, E. M., Oka, T., Vergados, J., *Phys. Lett.* B166: 274 (1986)
171. Green, A. M., Niskanen, J. A., Richard, J. M., *Phys. Lett.* B121: 101 (1983)
172. Richard, J. M., *Nucl. Phys. B. Proc. Suppl.* 8: 128 (1989)
173. Baillon, P., et al., *Nuovo Cimento* A50: 393 (1967)
174. Armenteros, R., et al., *Phys. Lett.* 9: 207 (1964)
175. Maglic, B. C., et al., *Phys. Rev. Lett.* 7: 178 (1961)
176. d'Andlau, C., et al., *Phys. Lett.* 17: 347 (1965)
177. Alde, D., et al., *Phys. Lett.* B205: 397 (1988)
178. Baumgartner, B., Grosse, H., Martin, A., *Nucl. Phys.* B254: 528 (1985); Martin, A., Stubbe, J., *Europhys. Lett.* 14: 287 (1991)
179. Høgaasen, H., Richard, J. M., *Phys. Lett.* B124: 520 (1983)
180. Weinstein, J., Isgur, N., *Phys. Rev. Lett.* 48: 659 (1982); *Phys. Rev.* D27: 588 (1983)
181. Boutcmeur, M., Poulet, M., In *Hadron '89*, ed. F. Binon et al. Gif-sur-Yvette: Ed. Frontières (1989), p. 119
182. Aston, D., et al., *Nucl. Phys.* B301: 525 (1988)
183. Alde, D., et al., *Phys. Lett.* B201: 160 (1988); B198: 286 (1987)
184. Aston, D., et al., *Phys. Lett.* B201: 573 (1988)
185. Chung, S. U., et al., *Phys. Rev. Lett.* 55: 779 (1985)
186. Ando, A., et al., *Phys. Rev. Lett.* 57: 1296 (1986)
187. Dionisi, C., et al., *Nucl. Phys.* B169: 1 (1980)
188. Armstrong, T. A., et al., *Phys. Lett.* B221: 216 (1989)
189. Aihara, H., et al., *Phys. Lett.* B209: 107 (1988)
190. Bai, Z., et al., *Phys. Rev. Lett.* 65: 2507 (1990)

191. Duch, K. D., et al., *Z. Phys.* C45: 223 (1989)
192. Amsler, C., *Nucl. Phys.* A508: 501c (1990)
193. Bridges, D., et al., *Phys. Rev. Lett.* 57: 1534 (1986); 56: 211 (1986)
194. Ahmad, S., et al., In *Physics at LEAR with Low Energy Antiprotons*, Nucl. Sci. Res. Conf. Ser., ed. C. Amsler et al. Chur: Harwood Academic (1988), p. 447
195. Kolybasov, V. M., Shapiro, I. S., Sokolskikh, Y. N., *Phys. Lett.* B222: 135 (1989)
196. Riedlberger, J., et al., *Phys. Rev.* C40: 2717 (1989)
197. Angelopoulos, A., et al., *Phys. Lett.* B212: 129 (1988)
198. Gray, L., et al., *Phys. Rev. Lett.* 30: 1091 (1973)
199. Defoix, C., Espigat, P., CERN Yellow Rep. 74-18: 28 (1974)
200. Aker, E., et al., *Phys. Lett.* B260: 249 (1991)
201. Aker, E., et al., Submitted to *Nucl. Instrum. Methods* (1991)
202. Au, K. L., Morgan, D., Pennington, M. R., *Phys. Rev.* D35: 1633 (1987)
203. Longacre, R. S., et al., *Phys. Lett.* B177: 223 (1986)
204. Devons, S., et al., *Phys. Lett.* B47: 271 (1973)
205. Godfrey, S., Isgur, N., *Phys. Rev.* D32: 189 (1985)
206. Jaffe, R. L., *Phys. Rev.* D15: 267 (1977)
207. Diaz, J., et al., *Nucl. Phys.* B16: 239 (1970)
208. Daftari, I., et al., *Phys. Rev. Lett.* 58: 859 (1987)
209. Bassompierre, G., et al., *Phys. Lett.* B65: 397 (1976)
210. Guaraldo, C., *Nuovo Cimento* A102: 1137 (1989)
211. Cugnon, J., Vandermeulen, J., *Ann. Phys. Fr.* 14: 49 (1989)
212. Dover, C. B., In *1st Workshop on Intense Hadron Facilities and Antiproton Physics*, ed. T. Bressani et al. Bologna: SIF (1989), p. 55
213. Rafelski, J., *Phys. Lett.* B91: 281 (1980)
214. Dolgolenko, A., et al., See Ref. 40, p. 205
215. Cugnon, J., Deneye, P., Vandermeulen, J., *Phys. Rev.* C41: 1701 (1990); *Nucl. Phys.* A517: 533 (1990); Vandermeulen, J., Private communication
216. Kharzeev, D. E., Sapozhnikov, M. G., See Ref. 40, p. 59
217. Smith, G. A., See Ref. 104, p. 219
218. Bizzarri, R., et al., *Lett. Nuovo Cimento* 2: 431 (1969)
219. Oset, E., Hernandez, E., See Ref. 194, p. 753
220. Kondratyuk, L. A., Sapozhnikov, M. G., *Phys. Lett.* B220: 333 (1989)
221. Haeberli, W., See Ref. 194, p. 195
222. Armstrong, T., et al., *Phys. Rev.* D36: 659 (1987)
223. Mutchler, G. S., et al., *Phys. Rev.* D38: 742 (1988)
224. Dover, C. B., Richard, J. M., *Phys. Rev.* C25: 1952 (1982)
225. Dulude, R. S., et al., *Phys. Lett.* B79: 329 (1978)
226. Martin, A. D., Pennington, M. R., *Nucl. Phys.* B169: 216 (1980)
227. Hasenfratz, P., et al., *Phys. Lett.* B95: 299 (1980)
228. Brodsky, S. J., See Ref. 40, p. 15
229. Brodsky, S. J., Mueller, A. H., *Phys. Lett.* B206: 685 (1988)